

This is an Open Access document downloaded from ORCA, Cardiff University's institutional repository:<https://orca.cardiff.ac.uk/id/eprint/95585/>

This is the author's version of a work that was submitted to / accepted for publication.

Citation for final published version:

Darlington, Vicki, Blenkinsop, Thomas G. , Dirks, Paul, Salisbury, Jess and Tomkins, Andrew 2016. The Lawn Hill annulus: An Ordovician meteorite impact into water-saturated dolomite. *Meteoritics and Planetary Science* 10.1111/maps.12734

Publishers page: <http://dx.doi.org/10.1111/maps.12734>

Please note:

Changes made as a result of publishing processes such as copy-editing, formatting and page numbers may not be reflected in this version. For the definitive version of this publication, please refer to the published source. You are advised to consult the publisher's version if you wish to cite this paper.

This version is being made available in accordance with publisher policies. See <http://orca.cf.ac.uk/policies.html> for usage policies. Copyright and moral rights for publications made available in ORCA are retained by the copyright holders.



# The Lawn Hill annulus: An Ordovician meteorite impact into water-saturated dolomite.

Vicki DARLINGTON<sup>1\*</sup>, Tom BLENKINSOP<sup>1, 2</sup>, Paul DIRKS<sup>1</sup>, Jess SALISBURY<sup>3</sup> and Andy TOMKINS<sup>3</sup>

<sup>1</sup>College of Science and Engineering, James Cook University

<sup>2</sup>School of Earth and Ocean Science, Cardiff University

<sup>3</sup>School of Geosciences, Monash University.

\*Corresponding author: vicki.darlington@my.jcu.edu.au

**Abstract** – The Lawn Hill Impact Structure (LHIS) is located 250 km N of Mt Isa in NW Queensland, Australia, and is marked by a highly deformed dolomite annulus with an outer diameter of ~18 km, overlying low-metamorphic grade siltstone, sandstone and shale, along the NE margin of the Georgina Basin. This study provides detailed field observations from sections of the Lawn Hill annulus and adjacent areas that demonstrate a clear link between the deformation of the dolomite and the Lawn Hill impact. <sup>40</sup>Ar-<sup>39</sup>Ar dating of impact-related melt particles provides a time of impact in the Ordovician (472 ± 8 Ma) when the Georgina Basin was an active depocentre. The timing and stratigraphic thickness of the dolomite sequence in the annulus suggest that there was possibly up to 300 m of additional sedimentary rocks on top of the currently exposed Thornton Limestone at the time of impact. The exposed annulus is remarkably well preserved, with preservation attributed to post-impact sedimentation. The LHIS has an atypical crater morphology with no central uplift. The heterogeneous target materials at Lawn Hill were probably low-strength, porous and water-saturated, with all three properties affecting the crater morphology. The water-saturated nature of the carbonate unit at the time of impact is thought to have influenced the highly brecciated nature of the annulus, and restricted melt production. The impact timing raises the possibility that the Lawn Hill structure may be a member of a group of impacts resulting from an asteroid break-up that occurred in the mid-Ordovician (470 ± 6 Ma).

## INTRODUCTION

Meteorite impacts into carbonate-dominant, sedimentary targets are complex and poorly understood, because of the variable effects of porosity, water saturation and extreme heterogeneity of such target materials (Osinski et al., 2008). Each of these properties may alter the physical and chemical responses to the extreme temperatures and pressures generated at impact, thereby influencing the crater morphology.

With carbonate rocks present in ~30% of known sedimentary impact structures (Osinski et al., 2008) it is important to assess the effects of meteorite impacts in carbonate-rich environments. Carbonate rocks commonly contain little or no siliciclastic material and quench rapidly after melting. This makes the determination of pressure and temperature conditions at an impact site difficult using classic shock metamorphic features (Huson et al., 2010) such as shock metamorphosed quartz (Grieve et al., 1996). In addition, carbonate rocks have a much more complex pore system than most siliclastic rocks (Moore, 2001). Dolomitization has the potential to increase porosity, which can be further enhanced by subsequent karst processes (Moore, 2001). Pore collapse in highly porous materials will limit crater growth by absorbing large amounts of shock wave energy (Wünnemann et al., 2006; Miljkovic et al., 2012), which results in higher post-shock temperatures and a reduction in the critical melting pressure (Wünnemann et al., 2008). Porous rocks may also contain large amounts of pore water, which after vaporization, can alter the crater morphology, reduce melt production and increase brecciation (Kieffer, 1971; Ormö et al., 2006). Crater morphology can be further altered by heterogeneities in the lithology such as pronounced layering (Haines, 2005; Collins et al., 2008; Kenkmann et al., 2010), with block formation and rotation linked to vibrations in layered target zones (e.g. Waqf as Suwwan and Upheaval Dome impact structures, Kenkmann et al., 2010). Rheological heterogeneity across layered sequences may also result in differential deformation responses during impact, such as variations in the effects of acoustic fluidization between different units (Collins & Melosh, 2003).

The Lawn Hill Impact Structure (LHIS) is located in NW Queensland, ~250 km N of Mt Isa, (Fig. 1) and is defined by an annulus of deformed dolomite surrounding a core, the Gum Hole Plain. The annulus has an outer diameter of ~18 km and consists of Cambrian dolomite, which unconformably rests on top of low-metamorphic grade Mesoproterozoic siltstone, sandstone and shale. The inner area is ~8 km in diameter and is devoid of a dolomite cover. The dolomite unit in the annulus is highly deformed and brecciated, whereas rocks belonging to the same stratigraphic unit in close vicinity to the impact structure are undeformed. The Gum Hole Plain within the annulus yields well-preserved shock features, such as shatter cones (Fig. 2), and quartz grains containing planar deformation lamellae (Stewart & Mitchell, 1987). Mesoproterozoic siltstone and carbonaceous shale in drill core samples from the centre of the structure also contain pseudotachylite and microdiamonds linked to impact (Salisbury et al., 2008). In contrast, no definitive shock features have been described from the intensely deformed dolomite units within the annulus, thereby raising the possibility that the deformed dolomite resulted from events unrelated to the impact (Stewart & Mitchell, 1987).

Several hypotheses have been proposed to explain the anomalous deformation of the dolomite (Rands, 1901), the presence of carbonate breccia dykes, and overturning of large scale breccia blocks within the annulus. These include: a “cryptoexplosion” (Hutton, 1992), tectonic deformation (Carter & Öpik, 1961; de Keyser & Cook, 1972; Szulc, 1992; Feltrin, 2006), collapse, solution or compaction brecciation due to karst effects (Sweet & Hutton, 1980; Wilson & Hutton, 1980), karstification, solution collapse in combination with fault reactivation (Feltrin et al., 2003; Agnew, 2004; Feltrin & Oliver, 2014) and extra-terrestrial

1 impact (Stewart & Mitchell, 1987; Shoemaker & Shoemaker, 1990, 1996; Denaro et al., 1999; Haines, 2005; Lindsay & Brasier,  
2 2006; Salisbury et al., 2008).

3 Literature on the Lawn Hill dolomite annulus provides evidence for a range of ages for the deformation events affecting the  
4 Lawn Hill area, stretching from the Mesoproterozoic (Shoemaker & Shoemaker, 1996; Andrews, 1998b) to the Late Devonian  
5 (Feltrin, 2006). The studies that suggest a tectonic origin for the annulus structure link deformation to the Alice Springs Orogeny  
6 (450 to 300 Ma, Haines et al., 2001) and movement during the Late Devonian (Agnew, 2004; Feltrin, 2006; Draper, 2007). Early  
7 proponents of an impact origin for the Lawn Hill structure suggested a Late Proterozoic to Early Cambrian origin, predating  
8 deposition of the dolomite (Stewart & Mitchell, 1987; Shoemaker & Shoemaker, 1996). Considering the distinct deformation  
9 patterns in the dolomite, Salisbury et al. (2008) suggested an age for the impact structure that coincided with dolomite deposition.

0 The SW edge of the LHS overlies the world-class Century Zn-Pb-Ag deposit (Fig.1, Geological Survey of Queensland,  
1 2011). It is not uncommon to find major mineral deposits in association with impact structures indicating links between impact  
2 events and mineralization (Grieve & Masaitis, 1994), with the Witwatersrand gold deposits distributed around the Vredefort  
3 Dome, and the Sudbury Ni deposits being the most notable examples (Reimold et al., 2005). Near Century mine, hydrothermal  
4 vein-type Zn-Pb mineralization extends W of the current pit, away from the rim of the annulus (see Figure 1 in Salisbury et al.,  
5 2008), and the deposit probably represents an impact modified ore deposit.

6 In previous studies the annulus has been described in a regional context (de Keyser & Cook, 1972), but no detailed structural  
7 analyses have been performed to clarify the origin of the deformation patterns within the dolomite and investigate if such patterns  
8 are consistent with an impact. This study provides detailed field observations from sections of the Lawn Hill annulus and adjacent  
9 areas (Fig. 1), with the aim of describing the unique structures in the annulus and providing definitive evidence that the  
0 deformation patterns are consistent with an impact structure. The detailed structural descriptions also place constraints on the  
1 nature of the impact.

## 2 REGIONAL GEOLOGY

3 The LHS is situated towards the N of the Mt Isa Inlier (Fig. 1) (Geological Survey of Queensland, 2011). This area features a  
4 complex network of faults dominated by the NW trending Termite Range Fault (Fig. 1), which is a 70 km long fault that abutts the  
5 SW edge of the annulus (Feltrin, 2006). This fault exerted a major influence on local sedimentation patterns prior to the Isan  
6 Orogeny (1590 to 1500 Ma, Betts et al., 1999).

7 The stratigraphy of this part of the Mt Isa Inlier comprises up to 8500 m of variably deformed clastic and sedimentary rocks  
8 that are part of the Isa superbasin sequence (Feltrin, 2006), overlying the Kamarga Volcanics (Andrews, 1998a). The McNamara  
9 Group forms the uppermost part of the superbasin sequence (Feltrin, 2006), and hosts the Century deposit. The Lawn Hill  
0 Formation occurs at the top of this group, and reaches a maximum thickness of 2200 m (Fig. 3, Andrews, 1998a). It comprises  
1 four members. The basal member consists of ~1500 m of carbonaceous shale with concretions. It is overlain by ~200 m of tuffite  
2 (defined by Andrews, 1998a) and thickly bedded sandstone, and ~1050 m of interspersed shale and siltstone. Around Lawn Hill  
3 the top of the Lawn Hill Formation is composed of 550-650 m of micaceous sandstone (the Widdallion Sandstone Member).

4 The Lawn Hill Formation is unconformably overlain by rocks of the Georgina Basin sequence (Fig. 1), which cover an area  
5 of 325,000 km<sup>2</sup> straddling the Northern Territory and Queensland border (Tucker et al., 1979). Rocks in the Georgina Basin are  
6 generally unmetamorphosed, and the basal rocks W of the LHS are essentially undeformed. Unconformities within the  
7 sequence have been interpreted to result from broad uplift, downwarping and erosion rather than faulting and folding (Smith,  
8 1967). In the LHS only the basal units of the Georgina Basin sequence are exposed.

9 The base of the Georgina Basin sequence consists of the Thornton Limestone, which in the Lawn Hill area is composed of  
0 thick-bedded dolostone and dolomitic limestone with layers and nodules of chert (Smith, 1972). The unit is vuggy with a high  
1 porosity, and acts as a source of water for the perennially flowing Gregory River (Opik et al., 1961; Kruse et al., 2013). The  
2 dolostones of the Thornton Limestone in the annulus of the LHS represent an outlier of the Georgina Basin (Fig. 1). Along the  
3 NE edge of the Georgina Basin, the unit has a thickness of ~20 m directly W of the annulus, and thickens to ~100 m, 50 km S of  
4 the Lawn Hill area (Opik et al., 1961; Smith, 1967). The Thornton Limestone is disconformably overlain by a 1-30 cm thick  
5 layer of limonite-stained stratiform stromatolite; the Bronco Stromatolith Bed (Fig. 3), which in turn is disconformably overlain  
6 by the Gowers Formation (Southgate, 1986). The Gowers Formation consists of phosphatic limestone and dolostone, and locally  
7 contains chert concretions (Southgate, 1986). It reaches a thickness of ~5 m in the Lawn Hill area (de Keyser and Cook, 1972;  
8 Southgate, 1986). The Gowers Formation is overlain by the Camooweal Dolostone Formation, which reaches a maximum  
9 thickness of ~170 m (Kruse et al., 2013), and consists of dolostone and dolomitic limestone that is lithologically similar to the  
0 Thornton Limestone, but contains no chert (Southgate and Shergold, 1991).

1 An estimate for the maximum age of the Thornton Limestone can be obtained from volcanics of the Kalkarindji Large  
2 Igneous Province (LIP) which have been dated at  $510.7 \pm 0.6$  Ma using U-Pb and <sup>40</sup>Ar/<sup>39</sup>Ar methods (Jourdan et al., 2014) and  
3 occur within 20 km of the impact site, where they are conformably overlain by the Thornton Limestone. Faunal remains within  
4 the overlying Gowers Formation provide a bio-chronological age for the deposit of 508 to 506 Ma (Southgate, 1986), and also  
5 provide a minimum age limit for the Thornton Limestone.

6 The Georgina Basin experienced two further periods of sedimentation after formation of the LHS (Tucker et al., 1979). The  
7 first, occurred during the Devonian and was limited to the S parts of the Basin, away from the LHS. The second occurred during

1 the Jurassic-Cretaceous and involved a period of marine transgression, which led to the deposition of two units around the impact  
2 site (Fig. 1). It has been estimated that sandstone of the early Cretaceous, Gilbert River Formation may have blanketed the area to  
3 an estimated thickness of 60-140 m (Smart et al., 1980), and was covered by intercalated sandstone-shale units of the early  
4 Cretaceous Mullaman Beds that may have reached a thickness of up to 150 m (Fig. 3, Munson et al., 2013). The youngest deposits  
5 exposed in the Lawn Hill area consist of colluvial and alluvial sediment of Quaternary age, grouped as the Armraynald Beds,  
6 which reach a thickness of up to 70 m (Langford et al., 1988). The Armraynald Beds are exposed across the Gum Hole Plain  
7 inside the annulus and extend N and NE along the river valleys away from the annulus (Fig. 1 and Fig. 2) (State of Queensland  
8 DNRM, 2011b).

## 9 METHODS

0 A series of mapping and geochemical techniques were applied in obtaining the data as detailed below.

### 1 Map compilation in GIS and Field Mapping

2 Geological and geographical digital maps of the Lawn Hill area were obtained from the Queensland and Northern Territory  
3 Geological surveys (Northern Territory Geological Survey DME, 2011; State of Queensland DNRM, 2011a, b). These maps were  
4 combined in ArcMAP 10.2 using the Geocentric Datum of Australia 1994 (GDA94). A Google Earth image of the area was used  
5 for geological interpretation (cf. Tewksbury et al., 2012), which together with the Queensland Globe imagery and terrain updates,  
6 were imported into ArcMAP. Additional geological data from maps at 1:100 000 and 1:250 000 scales (Bureau of Mineral  
7 Resources, 1982) were digitized and incorporated where appropriate. Regional field mapping was undertaken, with detailed  
8 mapping focused on two, 1 km-wide radial strips covering the E and NE sides of the annulus, the Mt Jennifer area, and three small  
9 outcrops of dolomite near the outer rim and to the S of the annulus structure (Southern Outcrops; Fig. 1), as well as outcrops of the  
0 Georgina Basin proper in parts of the Boodjamulla National Park (Fig. 1). Field data and geological maps have also been  
1 displayed in Google Earth (cf. Blenkinsop, 2012), together with additional photographs of critical outcrops and geological features  
2 of interest, which are included in the supplementary material. This additional material has been placed in folders/subfolders,  
3 named in reference to the manuscript section where they are first mentioned, followed by the position label, e.g. LHis.kmz/The  
4 Lawn Hill Annulus/Bronco Stromatolith/LH-408, -582, -583, -608 indicates photographs of stromatolites at four locations LH  
5 408, LH 582, LH 583 and LH 608 from the Bronco Stromatolith Bed located within the Lawn Hill Annulus.

### 6 Structural Analyses

7 Structural data (poles to bedding) were visualized using Stereonet version 8.0.2 (Allmendinger et al., 2011), and analyzed using  
8 a Bingham axial distribution function to determine normalized eigenvalues ( $\lambda_1, \lambda_2, \lambda_3$ ). These eigenvalues were used to calculate  
9 the corresponding fabric shape and strength (Vollmer, 1990), and to determine the point (P), girdle (G) or random (R) indices of  
0 fabric types. The intensity value (I) (Lisle, 1985) was used to compare the degree of preferred orientation between the different  
1 areas of interest and has been represented as contours on the ternary graph of Vollmer (1990).

### 2 Chemical staining techniques

3 Chemical staining of selected dolomite samples was undertaken using Alizarin Red S and potassium ferricyanide to determine  
4 the carbonate types present in the deformed dolomite and associated breccias (Ayan, 1965).

### 5 Geochemical Analyses

6 Electron probe microanalysis (EPMA) on matrix and clast material from selected breccia samples (LH101 and LH648; Fig. 1)  
7 was done using the JXA 8200 microprobe at the James Cook University Advanced Analytical Centre. Analyses were performed in  
8 WDS mode, using an accelerating voltage of 15 kV and a beam current of 20 nA. The electron beam was defocused to 5  $\mu\text{m}$ . The  
9 data were corrected using the ZAF procedure. Powdered clasts taken from sample LH101 were analyzed using EDS and  
0 XRD/XRF at James Cook University. A Siemens D5000 Diffractometer (XRD) with a theta-2 theta goniometer and a copper  
1 anode x-ray tube, fixed slits, monochromator and a forty position sample changer was used to identify the minerals. A Bruker-  
2 AXS S4 Pioneer X-ray Fluorescence Spectrometer with SpectraPlus software was used for XRF analyses.

3 EPMA was also applied to determine the composition of minerals for samples JS006 and JS023 that were used for dating.  
4 These analyses were performed at the University of Melbourne, using a Cameca SX50 in WDS mode, with an accelerating  
5 voltage of 15 kV and a beam current of 35/25 nA. The data were corrected using matrix correction software PAP (Pouchou &  
6 Pichoir, 1984) integrated into the SAMx software package (Thiot & Pouchou, 1996) used for automation and data reduction.

7 Analytical results are presented in the supplementary material (Tables S1-5) and these results are duplicated and presented  
8 within the Supplementary File, LHis.kmz/geochronology.

### 9 Dating techniques

0  $^{40}\text{Ar}$ - $^{39}\text{Ar}$  analyses were conducted at the University of Melbourne, using analytical procedures described by Phillips et al.  
1 (2004) and Phillips and Harris (2008) involving step-heating. A defocused  $\text{CO}_2$  laser was used to perform the step-heating  
2 procedure. Gas purification was achieved by means of two SAES NP10 getters, operated at 400°C and room temperature,  
3 respectively. A MM5400 mass spectrometer, equipped with a Daly detector, carried out Argon isotopic analyses. J-values were  
4 calculated relative to an age of  $98.8 \pm 0.5$  Ma for GA1550 biotite (Renne et al., 1998). Analyses of standard air volumes from a  
5 Nupro pipette system were applied to monitor mass discrimination. System blanks, mass discrimination, and radioactive decay of  
6  $^{39}\text{Ar}$  and  $^{37}\text{Ar}$ , and reactor interferences were corrected using extended line blanks (10-20 min). Demonstrated atmospheric  $^{40}\text{Ar}$ -

<sup>36</sup>Ar compositions (Renne et al., 2009), and reported argon isotopic data for <sup>40</sup>Ar-<sup>39</sup>Ar ages are additionally corrected for atmospheric contamination (assuming all <sup>36</sup>Ar is atmospheric), and fluence gradients. Unless otherwise stated, errors are given as 2σ, and exclude uncertainties in the J-values. Decay constants are those recommended in Steiger and Jäger (1977).

## STRUCTURES OF THE LAWN HILL IMPACT

### The Lawn Hill annulus

Cambrian dolomite at the LHS forms a ring-shaped map pattern referred to as the annulus (Fig. 1). Siliceous breccia is exposed along most of the inner edge of the annulus. The annulus is asymmetric in shape; with a width of ~7 km of dolomite preserved along the NE part of the annulus compared to ~1 km adjacent to Century mine (Fig. 1). The dolomite unit reaches a thickness of 200-400 m in the annulus (Lindsay & Brasier, 2006). Based on field data, estimated lithology thicknesses (Andrews, 1998b) and drill core information a section across the annulus has been reconstructed (Fig. 4). The dolomite is predominantly micritic with a combination of oosparite, oomicrite and biosparite in restricted areas. Oolitic patches contain both oncolites and peloids. Chert bands (mm- to cm-scale) or chert nodules occur interbedded with the dolomite. A layer containing fossil shells, possibly hyolithids (de Keyser & Cook, 1972), was found in isolated locations within 2 km of the outer edge of the annulus along the NE strip. The dolomite locally contains 5-50 cm thick beds with domal stromatolites (laterally linked hemispheroidal type; LLH Walter, 1972). Silicified, larger diameter (~30 cm) LLH stromatolites occur in the inner region along the E strip (Fig. 5). These larger stromatolite beds are comparable with the Bronco Stromatolith Bed found 100 km to the S of the LHS. Stromatolite beds with smaller diameter (~5 cm) LLH stromatolites occur on the outer edge along the NE strip. Oncolites can also be found as isolated clasts within the breccia along both the NE and E strip (Supplementary File, LHS.kmz/The Lawn Hill Annulus/Bronco Stromatolith: LH408, 582 and 3, 608). The Bronco Stromatolith Bed contains both stromatolites and oncolites. Some of the Bronco Stromatolith Bed stromatolites are characterized by a palisade structure, which is a feature of the smaller stromatolites seen at LHS.

The Lawn Hill annulus is folded, faulted and brecciated (Fig. 6), with clasts ranging from 1 mm to 100 m in size. Megaclasts contain coherent folds on a scale of 30-100 m (Fig. 6). Folds within individual megaclasts do not display constant orientations or systematic changes in orientation between clasts. Instead, the orientation of fold hinges, fold axial planes and bedding planes, varies in a random, non-systematic manner from one breccia block to the next. Boudins occur in chert layers found within the Thornton Limestone, which together with the folds indicate that the rocks were folded and boudinaged before the breccia blocks were formed (Supplementary File, LHS.kmz/Lawn Hill Annulus: LH136). Locally within the annulus, bedding planes are overturned, and bedding orientations range from horizontal to vertical. None of the deformation features seen within dolomite in the annulus occur in the Thornton Limestone (dolomite) as exposed in the Boodjamulla National Park less than 15 km to the W (Fig. 1), the N end of Mt Jennifer, or the S most parts of the Southern Outcrops to the S of the annulus where bedding is near horizontal. The N section of the Thornton Limestone at Mt Jennifer consists primarily of bioclastic limestone (Supplementary File, LHS.kmz/Mt Jennifer and the Southern Outcrops: LH2 763).

Stereoplots of poles to bedding combining data from this study with data presented in Szulc (1992) show a dispersed distribution of bedding plane orientations around the horizontal (Fig. 7a-c). Bedding plane orientations taken from layers with known younging directions have been shown separately in Figure 7. The majority of the Szulc (1992) data, in the SW part of the annulus, lacks definitive way-up indicators (Fig. 7c) and only a few overturned beds were noted making the comparison between the data presented by Szulc (1992) and this study difficult. The paucity of stromatolite beds along the NE strip (Fig. 1) also reduced the ability to identify definitive way-up indicators. Outcrops along the E strip (Fig. 1) contain stromatolite beds throughout, thus facilitating the determination of way-up criteria. In this area, upright and overturned bedding planes were observed to occur at a similar frequency. A fabric strength analysis for the datasets obtained from the NE, E, and SW parts of the annulus indicate a uni-axial strain distribution pattern with  $\lambda_2$  being near equal to  $\lambda_3$  (Fig. 8) (Vollmer, 1990). The eigenvalues calculated for the datasets indicate that the distribution pattern of bedding planes along the NE strip and SW domain are geometrically similar.

The E and NE strips have been subdivided into inner, middle and outer sections, based on an observed variation in the dominance of breccia in the middle section of both strips. The middle section is approximately 2.7 km from the inner edge of the dolomite and covers an area of 1 km<sup>2</sup> along both strips. The three sections in the E strip (inner, middle and, outer) display a larger range in fabric orientations and fabric intensity than the sections along the NE strip (Fig. 8). The entire SW domain is comparable to the middle section along the NE strip in terms of fabric distribution and intensity.

### Mt Jennifer and the Southern Outcrops

Mt Jennifer (Fig. 9a) is located 2 km NW of the outer edge of the Lawn Hill annulus. The dolomite along the S edge at Mt Jennifer consists of a nodular dolomite facies (Supplementary File, LHS.kmz/Mt Jennifer and the Southern Outcrops: LH2-798), similar to the outer edge of the annulus along the NE strip. Bedding planes within dolomite along the S edge of the Mt Jennifer area dip gently N, whereas elsewhere, bedding planes at Mt Jennifer are close to horizontal (Fig. 9a; Supplementary File, LHS.kmz/Mt Jennifer and the Southern Outcrops). The Widdallion Sandstone Member can be seen below the Thornton Limestone at Mt Jennifer.

The Southern Outcrops (Fig. 9b) lie 1 km SE of the outer edge of the Lawn Hill annulus, and consist of three small outcrops of Thornton Limestone (Fig. 1). These outcrops of dolomite have been designated inner, middle, and outer from NW to SE, i.e. away from the core of the annulus, and they mark the transition from deformed to undeformed dolomite. The inner outcrop marks the limit of the brecciation, but both the inner and middle outcrops display variable orientations of bedding with average dips of >

30°. The outer outcrop is predominantly horizontally bedded with a gentle southward dip ( $< 15^\circ$ ) occurring along its N edge (Fig. 9b). A large overturned LLH stromatolite bed occurs on the N edge of the inner outcrop (Fig. 9b, Supplementary File, LHis.kmz/Mt Jennifer and the Southern Outcrops: LH2-864). Less than 500 m to the E, stromatolitic limestone in the outer outcrop shows no variation in orientation. Along the N edge of the outer outcrop, the unconformable contact between siltstone and Thornton Limestone is exposed. Thus, the outer margin of the annulus to the S is characterized by overturning of the dolomite beds.

## The Gum Hole Plain

The Mesoproterozoic rock exposures in the Gum Hole Plain (Fig. 2) are folded and fractured reflecting deformation patterns that are consistent with the regional deformation events preserved within these basement rocks; e.g. sandstone units display parallel folds with interlimb angles ranging from tight to open. There are no highly fractured zones that display large-scale rotation of blocks or breccias. The basal unit of the Lawn Hill Formation is recognized by the presence of concretions. Concretions are found at LH-026 ( $18^\circ44'24.30''S$ ,  $138^\circ42'18.24''E$ ), as well as on the surface of Gum Hole Plain but the concretions found within the Gum Hole Plain are predominantly fractured. Folding and melt-like features are present in sandstone and siltstone units exposed in the centre of the Gum Hole Plain (Fig. 10a-c), with some samples displaying flow textures. This melt material is described in detail by Stewart and Mitchell (1987) Ashley (2010) described similar material from a drill core ( $18^\circ41'31.53''S$ ,  $138^\circ38'13.84''E$ ) as resembling rhyolite. The melt breccias are located within this drill core at 48, 69 and 106 m below the surface of the Gum Hole Plain. Fabric orientation of this melt material indicated no identifiable pattern however the poles of the hinge surfaces are all directed NW-NE. The region of melt rocks identified in this study is comparable to that previously mapped (see Figure 16 in Shoemaker & Shoemaker, 1996). However, evidence of melt material in the drill core from LH-355 suggests that the melt region is larger than that shown.

*In-situ* shatter cones are located in two areas: 1)  $\sim 1.9$  km NNE of the centre of Gum Hole Plain ( $18^\circ40'39''S$ ,  $138^\circ39'37''E$ ) and 2)  $\sim 1.4$  km NE of the centre of the Plain (Fig. 2,  $18^\circ41'23''S$ ,  $138^\circ39'49''E$ ). A band of Proterozoic rocks within the NNE part of the Gum Hole Plain (Fig. 2) contains classic horsetail striations (Dietz, 1959; Manton, 1965) interpreted as shatter cones. These outcrops show that the extent of rocks that preserve shatter cones is larger than the area recorded by Stewart and Mitchell (1987) (Fig. 2). Siltstone with shatter cones is also found around the outer edge of the melt rocks near the impact centre. *In-situ* shatter cones have been found in siltstone, mudstone, and sandstone (Supplementary File, LHis.kmz/The Gum Hole Plain: LH2-754,-762,-971 and -974). Shatter cones in siltstone display more clearly defined striations than those preserved in mudstone. Apex orientations of shatter cones vary by up to  $180^\circ$  on adjacent *in-situ* surfaces as well as on different surfaces within single cobbles (Fig. 11, Supplementary File, LHis.kmz/The Gum Hole Plain). The majority of apex orientations point outward, i.e. away from the impact centre (Supplementary File, LHis.kmz/The Gum Hole Plain).

Cobbles with shatter cones (Fig. 2) are located in the NE and E sector of the Gum Hole Plain. A small number of cobbles, with shatter cone striations have also been found in the S part of Gum Hole Plain, but such cobbles have well-rounded edges suggesting transportation. Cobbles containing cone-in-cone structures and small concretions are present at the impact site. These were found in the Gum Hole Plain and in the colluvium outside the dolomite annulus. Microstructural analysis eliminated any possible confusion between concretion, cone-in-cone structures and shatter cones (Sellés-Martínez, 1996; Lugli et al., 2005).

## Breccias

Meso-scale breccias are a distinct feature within rock outcrops of the annulus, Gum Hole Plain and the nearby Mt Jennifer area. The various breccia units present in the Lawn Hill area fall into 2 classes: 1) dolomite-chert breccia in a calcitic matrix and 2) sandstone-quartz breccia in a siliceous matrix.

### Dolomite-chert breccia

Dolomite-chert breccia forms beds or masses throughout the mega-clastic dolomite blocks (Fig. 12a-c) in the annulus. Contacts between breccia and intact dolomite can be either sharp or gradational, with masses of breccia crosscutting bedding. Pockets of breccia cover areas up to  $3000\text{ m}^2$  in extent and range in thicknesses from 0.1 to 10 m. Diamond drilling through the dolomite annulus indicates that the contact between basement and cover is characterized by extensive brecciation and a 20-30 m wide zone in which Meso-Proterozoic basement rocks are interleaved with dolomite (Salisbury et al., 2008). The breccia contains both chert and dolomite clasts ranging in size from 2 to 500 mm. Only the chert clasts were found to be smaller than 5 mm in size, whereas dolomite dominates the clasts that are larger than 200 mm. The larger dolomite clasts can contain thin chert layers that are common in the deformed dolomite blocks in the annulus. The dolomite-chert breccia in the annulus locally contains small ( $< 1\%$ ) clasts composed of a white powdery material with a composition dominated by Si, Ca, Al, and Mg with minor Cl, P, and K. XRD analyses indicate the presence of kaolinite, dolomite ( $> 40\%$  each) and quartz (10%) (Table S3). These clasts have been interpreted as the remains of dolocrete and may have formed a crust covering the dolomite at the time of impact. Within the annulus breccia is generally poorly sorted and matrix supported, with local fining upwards of clast size (Fig. 1 and Fig. 12a-c; Supplementary File, LHis.kmz/Annulus breccia: LH-101, LH-648, LH-620). Staining suggests the matrix material is calcite rather than dolomite, but microprobe analyses indicate there is no difference between the MgO and CaO quantities in the dolomite clasts and the calcite matrix for those samples that were analysed (combined average 21.3 % MgO, 28.5 % CaO, 15 samples; Tables S1 and S2). None of the chert clasts within the samples viewed in thin section contains shock features.

Two other dolomite-chert breccia types are found associated with the impact event. The Thornton Limestone at Mt Jennifer hosts a breccia (Fig. 12d, Supplementary File, LHis.kmz/Mt Jennifer breccias: LH2-800, -802, -803, -786) similar in appearance to the dolomite-chert breccia in the annulus. This breccia type, however, occurs in sub-vertical dykes up to 100 m in length and up

to 0.5 m wide (Fig. 12d). This breccia preserves a variable clast to matrix ratio (80:20 to 30:70) with clasts generally consisting of a combination of dolomite and chert. One dyke (Supplementary File, LHis.kmz/Mt Jennifer breccias: LH2-786) also contains sandstone clasts from the Widdallion Sandstone Member. A further dolomitic breccia type is located towards the N edge of the Gum Hole Plain (Fig. 13a, LHis.kmz/GHP breccia: LH-183). This breccia has a high clast to matrix ratio with two generations of fracturing in the clasts. Staining indicates the matrix material is calcite and that the breccia is matrix supported.

### **Sandstone breccia in a siliceous matrix**

Sandstone breccia in a siliceous matrix occurs in outcrops near Mt Jennifer and along the boundary zone between the Gum Hole Plain and the annulus (Fig. 13c; Supplementary File, LHis.kmz/Mt Jennifer breccias and Annulus breccias: LH2-850, -849, LH-134). The siliceous breccia at Mt Jennifer occurs in sill-like masses located between beds of sandstone and siltstone. These breccia layers are ~50 cm thick at the S end of Mt Jennifer where they occur in multiple subvertical layers separated by ~1 m thick zones of intact sandstone/siltstone. This type of breccia is also present 300 m NW of the Mt Jennifer breccia sills (18°36'26"S, 138°35'41"E) (Fig. 1). The outcrops of breccia along the outer edge of the Gum Hole Plain are massive (5-50 m in length), and have comparable textures to the siliceous breccia at Mt Jennifer. This breccia contains angular (90 %) and rounded (10 %) clasts, with a vuggy matrix. The sandstone unit exposed below the Thornton Limestone (18°36'12"S, 138°35'28"E) has material that is locally brecciated (Fig. 13b; Supplementary File, LHis.kmz/Mt Jennifer breccias: LH2-770) with a high clast to matrix ratio.

## **GEOCHRONOLOGY**

Two samples have been collected for <sup>40</sup>Ar-<sup>39</sup>Ar analysis; sample JS-006 from drill core and sample JS-023 from a surface outcrop (Fig. 2). A binocular microscope was used to handpick sample JS-006 from impact melt particles (fragments > 3 mm) and K-feldspar spherules (< 0.1 mm) from a 15 cm interval at 172.7 m depth in a diamond drill hole LH-355, drilled into the centre of the structure, containing spherules in partially melted carbonaceous shale and siltstone. The fluidal melt domain features dark convoluted and contorted particles with embedded siltstone breccia fragments (Fig. 14). Spherules are present, but rare in the darker areas of the melt, which mostly consist of quartz and some calcite, with minor calcite space-fill and quartz veining throughout the sample (Fig. 15).

Electron microprobe analysis of the fluidal melt domain gave an average potassium content of ~3%, which is sufficient for <sup>40</sup>Ar-<sup>39</sup>Ar analysis (Table S4 and S5). Sample JS-023 was obtained from dark, melt-rich domains in a surface specimen collected from close to the centre of the Gum Hole Plain. The sample contains convoluted recrystallized impact melt material encasing 4-5 mm large K-feldspar spherules (Fig. 15) with fine-grained radial striations indicative of rapid cooling. Optical petrography and electron microprobe analysis of the spherules indicate that the dark bands are composed of K-feldspar (sanidine) set in a matrix of fine-grained quartz (~0.3 mm grain size), indicative of high temperature crystallization (Sharp et al., 1992) (Supplementary File, LHis.kmz/Geochronology; JS-006).

Isoplot was used to analyze the <sup>40</sup>Ar-<sup>39</sup>Ar data (Table 1, Fig. 16a and b). Sample JS-006 exhibits two plateaus at mean ages of 483.63 ± 0.94 Ma, and 457.7 ± 1.5 Ma (Fig. 16a), which is most likely due to partial devitrification of the impact melt particles, resulting in higher recoil loss and more redistribution of <sup>39</sup>Ar during irradiation than would otherwise be expected in homogeneous fluidal melt particles. Compositional variation such as this could result in anomalously old plateau ages, and multiple plateaus, which may account for the older plateau age (Ferguson & Phillips, 2001). A more accurate representation of the overall age of this sample, despite the higher possible error, is the integrated total gas age at 472.3 ± 8.0 Ma. Sample JS-023 exhibits one plateau with a mean age at 477.90 ± 0.76 Ma (Fig. 16b), which is not reported as a plateau age, as this represents < 60 % of released <sup>39</sup>Ar. However, the stabilization of the heating curve at this point, suggests that the mean age is the best reflection of the sample age. The broadly similar heating curves and agreement in age results provide confidence in the ages reported, especially considering that compositionally different sample material was used.

## **DISCUSSION**

### **The origin of the Lawn Hill annulus**

Because the dolomitic rocks of the annulus at Lawn Hill do not contain unambiguous textures indicative of an impact origin (e.g. shatter cones, deformation lamellae, high-P mineral phases, pseudotachylite veins and melt), even though they surround a known impact site (Stewart & Mitchell, 1987), a wide range of alternative models have been proposed to explain the structure (Carter & Öpik, 1961; de Keyser & Cook, 1972; Sweet & Hutton, 1980; Wilson & Hutton, 1980; Szulc, 1992; Feltrin et al., 2003; Agnew, 2004; Feltrin, 2006; Feltrin & Oliver, 2014). The validity of such models hinges on a detailed understanding of the deformation patterns assisted by accurate dating of the impact, both of which are provided in this paper.

A review of earlier models demonstrates that it is hard to explain the localized, extremely high strain deformation pattern of the annulus by involving either tectonic or sedimentary processes, both of which would operate on a regional scale. Deformation patterns within the annulus at Lawn Hill are complex and restricted in areal extent. In contrast to the rocks of the annulus, the sedimentary rocks of the nearby Georgina Basin are flat lying and largely undeformed. Although Szulc (1992) suggested that some of the structures in the annulus may be attributed to regional deformation events, his interpretation was based on limited mapping. Our mapping across the full extent of the annulus on the NE and E sides clearly demonstrates the localized (Fig. 5), circular extent of the deformation patterns in the annulus, and the sharp outer boundary of the structure across which bedding planes resume a horizontal position. Therefore, the annulus must have formed due a highly localized deformation process in the absence of a significant, regional far-field stress.

1 One way to explain the localized nature of the annulus structure has been to invoke a variety of sedimentary processes. Firstly  
2 it has been suggested that the Lawn Hill impact occurred in the Mid-Cambrian (509-506 Ma), prior to deposition of the  
3 Thornton Limestone (Lindsay & Brasier, 2006). In this interpretation the thickening of the dolomite unit around the annulus has  
4 been attributed to infill of a crater, in which pre-existing topography was gradually smoothed over as sedimentation progressed.  
5 The intense brecciation of dolomite in the annulus structure has been attributed to gravity-driven deformation mechanisms  
6 involving solution and collapse of the dolomite plateau (Sweet & Hutton, 1980; Wilson & Hutton, 1980), a process that was  
7 invoked to occur in a highly restricted manner near the annulus (Feltrin and Oliver, 2014). In this context it must be noted that the  
8 Thornton Limestone has been described as vuggy, brecciated and fractured (Ambrose, 2006) as well as porous and water-logged  
9 (Feltrin & Oliver, 2014), but it does not display large block rotations anywhere outside of the annulus.

0 Estimates for the depositional age of the Thornton Limestone between 511 Ma (Jourdan et al., 2014) and 506 Ma  
1 (Southgate, 1986) suggest that the impact post-dated the Thornton Limestone by as much as 35 Ma, when considering the new  
2  $^{40}\text{Ar}$ - $^{39}\text{Ar}$  date of  $472.3 \pm 8.0$  Ma for the impact structure (Fig. 16). An age of impact younger than the Thornton Limestone is  
3 consistent with the presence of breccia injection veins into basement rocks near the annulus, and 'dykes' and sub horizontal 'sills'  
4 of dolomitic breccia in Mesoproterozoic rocks in the Century pit (see Figure 4F in Salisbury et al., 2008). Thus, the annulus  
5 structure and dolomitic breccias cannot be explained with an early timing of impact and subsequent localized karst processes, and  
6 the most logical explanation for the geometry and deformation patterns within the annulus is that they formed as a direct result of  
7 impact. In this case the nature of the structures in the annulus and their relationship with basement structures can be used to  
8 constrain the type of impact, and possibly the composition of impactor itself.

9 If the Thornton limestone was not deposited within a pre-existing crater, one characteristic that is hard to explain in an  
0 impact setting is the anomalous thickness of the dolomite stratigraphy that has been preserved in the annulus, which is up to  
1 twenty times that of the Thornton Limestone (i.e. ~20 to 100 m) as exposed in outcrops in the Georgina Basin, ~15 km to the W.  
2 Considering the presence of overturned rocks within the carbonate sequence in the annulus, and using available drill core data, we  
3 estimate that the total stratigraphic thickness of carbonate sediment at the impact site may have been as much as 250 to 300 m, i.e.  
4 significantly more than the maximum recorded thickness of the Thornton Limestone. The simplest way to explain this apparent  
5 anomaly is if the dolomite in the annulus is not just composed of Thornton Limestone, but also contains remnants of overlying  
6 units, including the Bronco Stromatolith bed, the Gowers Formation, and the Camooweal Dolostone. This is possible considering  
7 the near identical nature of these units to the Thornton Limestone, and the widespread presence of stromatolite beds and chert-  
8 free dolostone within the annulus. If so, this would constrain the timing of impact to sometime during or after deposition of the  
9 Camooweal Dolostone.

0 The LHS is well-preserved in spite of its age, and has not been eroded very deeply, with the dolomite unit that was most  
1 likely on surface when the impact took place, still present. One explanation for this preservation is that sedimentation continued  
2 after impact, with sediments blanketing the impact site, and halting significant erosion in a similar manner to the Deep Bay and  
3 Clearwater East impact structures (Dence, 2002). Remnants of Mesozoic rock units indicate that further blanketing of the site  
4 occurred during this period. Uplift and erosion during the Cenozoic will have gradually exposed the site, but low-topography and  
5 a dry climate would have contributed to slow erosion rates (Portenga & Bierman, 2011).

6 A Mid-Ordovician impact age for the Lawn Hill structure also means that it could be part of a larger flux of cratering events  
7 thought to have been generated at this time by the breakup of an asteroid in the asteroid belt at ~470 Ma (e.g. Schmitz et al.  
8 (2001). The current list of Mid-Ordovician impacts linked to this L-chondrite break-up stands at thirteen (Meinhold et al., 2011;  
9 Ormö et al., 2014; Schmieder et al., 2015), whereas modeling suggests that the Earth could have experienced up to 80 small  
0 asteroid (< 1 km diameter) impacts from this break-up over a 30 Myr time span (Zappalà et al., 1998). All of the current known  
1 structures linked to this event have been described from North America and the Baltic, whilst no coeval impact structures have yet  
2 been located on Gondwanaland, which represented about two-thirds the continental mass in this period (Smith, 1999). The  
3 identification of the LHS as Mid-Ordovician is, therefore, consistent with the expected abundance and likely world distribution of  
4 impact structures related to this event.

## 5 **The LHS and its constraints on the type of impact**

6 Few of the expected crater features associated with an ~18 km diameter impact structure appear to be present in the LHS. In  
7 contrast to most terrestrial impacts of this size the LHS shows no evidence for a central uplift within the Gum Hole Plain, or an  
8 uplifted crater rim with a marginal collapse zone and a high degree of symmetry (French, 1998). Likewise, impact melt lithologies  
9 and crosscutting pseudotachylite veins with allochthonous breccia, and subcrater rocks with a high degree of fracturing (French,  
0 1998) are largely absent across the Gum Hole Plain.

1 While Shoemaker and Shoemaker (1996) observed that the older sediments of the McNamara Group were folded prior to  
2 impact, they stated that the exposed siltstone and sandstone units of the Lawn Hill Formation in the Gum Hole Plain defined the  
3 outer edge of a central uplift. However, this basement material is only exposed on the NE side of the Gum Hole Plain and the  
4 deformation features in this area are entirely consistent with pre-impact deformation structures, and probably did not result from  
5 impact-related effects. Thus, although shatter cones are evident on some of the exposed rocks in the Gum Hole Plain, there is no  
6 measurable evidence of uplift, because the lithologies and structures exposed within the central area are similar to those exposed  
7 outside the annulus. The aeromagnetic (TMI) image of the LHS (see Fig 6b in Salisbury et al., 2008) also shows no anomalous  
8 structures that can be attributed to the impact.

1 Considering that the dolomite annulus at Lawn Hill is probably part of the overall impact structure, there appears to be a  
2 sharp contrast in the nature and intensity of impact related structures in the basement rocks as exposed in the Gum Hole Plain, and  
3 the intensely brecciated cover rocks exposed in the annulus. This contrast needs to be explained. Numerical modeling shows that  
4 impacts into layers of variable material strength and thickness have the capacity to localize deformation and alter crater  
5 morphologies (Senft & Stewart, 2007). It is the mismatch in acoustic impedance at the lithological boundaries that results in wave  
6 scattering, and the rapid dissipation of the shock wave energy (Zhuang et al., 2003; Chen & Chandra, 2004). Wave scattering at  
7 lithological boundaries can result in delamination (Chen & Chandra, 2004), which may explain the limited mixing across the  
8 lithological boundary at the LHis. Delamination along weak bedding planes was used to explain some of the deformation at the  
9 Chicxulub impact crater (Kenkmann et al., 2004). The Jebel Waqf as Suwwan impact structure in Jordan (Salameh et al., 2008;  
0 Kenkmann et al., 2010) has a lithologically similar setting to the LHis, with limestone resting upon a basement of sandstone,  
1 noting there is no mention of water saturation. This impact structure is 6 km in diameter and preserves a ring syncline containing  
2 block-faulted lithologies displaying micro- to meso-scale faulting, and a central zone with stratigraphic uplift that is considerably  
3 less than expected. The heterogeneity in the lithological sequence at the Jebel Waqf as Suwwan impact structure has been  
4 identified as a key influence on the folding and block faulting with weak layers restricting the transfer of energy across to more  
5 competent layers (Kenkmann et al., 2010). This phenomenon may also explain why the distinctive folding and faulting pattern  
6 within the annulus is absent from the basement sediments at the LHis. The lack of central uplift at LHis may indicate a greater  
7 mismatch in acoustic impedance at LHis compared to that of Jebel Waqf as Suwwan impact structure.

8 In addition to the effects of layered target lithologies, the rheological properties of the projectile itself must also be considered  
9 in explaining the anomalous nature of the LHis. To explain the lack of central uplift and a clear crater rim it could be suggested  
0 that the meteorite had a small diameter or a low velocity resulting in limited penetration. However, these combinations are  
1 unlikely to produce an impact structure of the magnitude and size of Lawn Hill. A low-density, high-velocity meteorite; i.e. a  
2 comet may need to be considered. While comets have been identified to travel at higher velocities (ave. 32 km/s; Hughes &  
3 Williams, 2000) their total energy is low because the average comet density is ca 500 kg/m<sup>3</sup> (Solem, 1994) compared with known  
4 lunar meteorites that have a measured density in the range of 2850-3300 kg/m<sup>3</sup> (Macke et al., 2011). To take this work further  
5 detailed modeling is required to test the validity of these various scenarios.

## 6 **Brecciation of the annulus as a result of hydrofracturing of water-saturated dolomite**

7 Rapid energy dissipation at the Lawn Hill impact site may explain the failure to form a central uplift. The intense brecciation  
8 across a large area of the dolomitic cover sequence, however, requires a further deformation mechanism linked to layered  
9 sediments; i.e. hydro-fracturing. The carbonate cover sequence in the Lawn Hill area has been identified as both porous and a  
0 source of groundwater (Megirian, 1992). Although the breccia contains clasts interpreted as dolocrete, which suggests that at the  
1 time of impact the land surface was above water, it is quite possible that the dolomite sequence was water-logged.

2 The boundary between the water-saturated Thornton Limestone and impermeable Widdallion Sandstone member may have  
3 had a significant influence on shock wave propagation with any water present in the dolomite expected to have vaporized and  
4 expanded outward (Ormö et al., 2006). Two physical experiments show the effects of water driven horizontally from an impact  
5 site. Water was found to generate geyser-like structures ahead of the shock wave (Ormö et al., 2006), and block-like fracturing  
6 occurred as saturation levels increased (Rager et al., 2014). This water spray may have resulted in fluidization, instabilities and  
7 site dewatering ahead of the impact shock wave in the area outside the transient crater. This scenario is evidenced by the  
8 brecciation ahead of the shock wave followed by block rotation present within the annulus.

9 Alternatively the brecciation could be a result of water vaporization following the shock wave during the rarefaction phase.  
0 Water vaporizes during the release phase if the pressure is above 5 GPa (Kieffer et al., 1976). In either scenario the behavior of  
1 water has been found to control that of rock (Kieffer et al., 1976). The presence of unmixed breccia throughout the annulus may  
2 mark the exit path of the water vapor through the weakened carbonate cover with the degree of fragmentation in breccias  
3 dependent on the quantity of water present (Rager et al., 2014). The dykes at Mt Jennifer appear to have formed along bedding  
4 planes and in vertical fissures in the dolomite. Alignment between the clasts and dyke wall occurs in the breccia with the lowest  
5 clast/matrix ratio. A likely source of the clasts is the abundant chert nodule beds, found throughout the Thornton Limestone at  
6 Mt Jennifer. These clastic dyke injections may have originated at impact as water-soaked, fluidized debris, injected at high speed  
7 as the fissures formed, in a similar fashion to the dykes at the marine Lockne impact structure (Sturkell & Ormo, 1997).

8 The superheated water that pushed out horizontally through the dolomite cover sequences may have also anomalously  
9 increased the annulus diameter and interrupted the process that normally results in the formation of a symmetrical crater (Melosh,  
0 1989). The asymmetrical nature of the annulus as defined by the dimensions of its outer rim could be evidence of site erosion;  
1 however, it may also be explained by dewatering. The presence of the Termite Range Fault on the SW side of the annulus may  
2 have provided a major conduit for escaping water vapor limiting both the brecciation and block rotation of the cover on the SE  
3 side of the annulus. The unusual presence of the large block of overturned stromatolitic dolomite in the Century mine pit  
4 (Salisbury et al., 2008) and a second block outside the current limits of the annulus at the inner S outcrop (Fig. 7) may indicate a  
5 major exit path for this heated water. This superheated water may have also been responsible for the high-magnesium calcite  
6 matrix, by providing the heat to melt the dolomite source material and the confined environment to prevent the escape of Mg<sup>2+</sup>,  
7 incorporating it in the calcite lattice (Jiang et al., 2011).

8 A marginal collapse zone is usually present in most terrestrial craters, with the width of the terracing increasing with distance  
9 from the impact centre, coupled with outwardly dipping surfaces (French, 1998). The meso- to macro-boulders found in the  
0 annulus at Lawn Hill do not increase in size towards the outer edge of the annulus. There is no identifiable terracing at the LHis.

1 Bedding orientations across the annulus are scattered around an average horizontal orientation with an equal proportion of upright  
2 and overturned bedding planes where these directions can be reliably determined (Fig. 9b). The random distribution of the blocks  
3 indicates a formation mechanism that is atypical of sedimentary impacts.

4 The Gum Hole Plain, in the core of the impact structure, represents the area where large quantities of melt breccias and melt  
5 rocks (e.g., in a melt sheet) would normally be expected (French, 1998) with melt production enhanced by material porosity  
6 (Wünnemann et al., 2008). While drill core indicates the presence of buried melt material there appears to be only low volumes of  
7 melt material at the LHis. This may be explained by erosion, however the dolomite annulus appears to have experienced minimal  
8 erosion making it unlikely that the Mesoproterozoic sandstones and siltstones within the Gum Hole Plain would have fared  
9 differently. The presence of groundwater within the dolomite cover may have reduced melt production at the Lawn Hill impact  
0 site. Impact sites with saturated sediments produced similar outcomes to shallow water impacts (Ormö et al., 2006) and melt  
1 production in shallow marine impacts is minor (Dypvik et al., 2004). We suggest that the presence of groundwater within the  
2 porous dolomite cover increased energy dissipation upon impact resulting in limited melt production. This suggestion needs to be  
3 qualified by the observation that Pleistocene sediments cover much of the Gum Hole Plain, so the extent of impact melt may have  
4 been underestimated.

## 5 CONCLUSION

6 The intense deformation of the dolomite cover sequence in the Lawn Hill annulus was caused by the Lawn Hill impact. The  
7 situation of a highly deformed annulus surrounding a known impact site combined with a complete lack of deformation in  
8 equivalent sedimentary rocks outcropping just 15 km away and throughout a regional basin, provides a compelling set of  
9 geological circumstances that argue for an impact origin for the structures in the annulus.

0 The impact timing ( $472 \pm 8$  Ma) in the Mid-Ordovician suggests that the target Thornton Limestone (Middle Cambrian) was  
1 lithified and that there were probably up to 200 m of additional sedimentary rocks on top of the Thornton Limestone. The  
2 presence of overturned stromatolite beds present in the annulus suggests that the Bronco Stromatolith Bed extended to this  
3 location. The similarity of the Camooweal Dolostone to the Thornton Limestone and the severe deformation of the annulus  
4 material make differentiating between the Thornton Limestone and younger Camooweal Dolostone difficult, but it is likely that  
5 the Camooweal Dolostone was part of the target stratigraphy at the time of impact. The Mid-Ordovician impact timing makes the  
6 LHis a candidate for the group of impacts linked to the asteroid break-up and subsequent influx of L-chondrite meteorites striking  
7 Earth at this time. The exposed annulus appears remarkably well preserved considering the impact timing. The preservation has  
8 been attributed to post-impact sedimentation providing a protective layer until recent times.

9 The Lawn Hill impact has an atypical crater morphology. A typical impact of this size should have generated a central uplift,  
0 yet such structure is absent at Lawn Hill with the exposed lithologies and structures in the central area being similar to those found  
1 outside the annulus. The failure to form or maintain these features suggests extremely rapid dissipation of impact energy. The  
2 Lawn Hill target materials were heterogeneous, and we suggest that some target units (i.e. the dolomite) were porous and  
3 contained large quantities of groundwater. Vaporization of this water and the associated hydrofracturing can explain the extent  
4 and intensity of brecciation observed within the dolomite of the annulus. The water-saturated dolomite layer, which occurred as a  
5 cover sequence overlying less permeable and deformed basement sediments may have dissipated energy rapidly in a downward  
6 direction, but may have enhanced damage in a horizontal direction as the shockwave was deflected along the lithological  
7 interface. Likewise, the presence of less permeable sandstone below the carbonate may have restricted crater depth but enhanced  
8 the diameter of the damage zone on surface. The presence of a water-saturated dolomite cover sequence at the time of impact is  
9 also consistent with the low amount of impact melt, the brecciated character of the annulus, and the presence of calcite matrix in  
0 the breccia.

1 *Acknowledgements:* We would like to thank Australian Geographic and the College of Science and Engineering (JCU) who  
2 have helped fund this research, and MMG Pty. Ltd. Century Mine staff for allowing access to the study area and providing  
3 logistical support. VD would also like to thank her husband, Anthony Darlington who happily became her field assistant for all of  
4 the fieldwork undertaken.

## 6 REFERENCES

- 7 Agnew, P. D. (2004). Century Zn-Pb-Ag deposit, northwest Queensland (pp. 3). 1 Research Ave, Bundoora, VIC, 3083: Rio Tinto  
8 Exploration Pty Ltd.
- 9 Allmendinger, R. W., Cardozo, N., & Fisher, D. M. (2011). Structural Geology Algorithms Vectors and Tensors. from  
0 <http://www.jcu.eblib.com.au/patron/FullRecord.aspx?p=824466>
- 1 Ambrose, G. (2006). The Georgina Basin 2006. In G. Ambrose & P. E. Putnam (Eds.), *Northern Territory of Australia, onshore*  
2 *hydrocarbon potential, 2006* (pp. 22). Darwin: Northern Territory Geological Survey.
- 3 Andrews, S. J. (1998a). *The regional setting of base metal mineralisation in the Middle Proterozoic Upper McNamara Group*  
4 *Lawn Hill Region NW Queensland Australia*. (PhD), University of Queensland, St Lucia, Qld.
- 5 Andrews, S. J. (1998b). Stratigraphy and depositional setting of the upper McNamara Group, Lawn Hills region, Northwest  
6 Queensland. *Economic Geology*, 93(8), 1132-1152. doi: 10.2113/gsecongeo.93.8.1132
- 7 Ashley, P. (2010). Petrographic report on three drill core samples and three rock samples from the Century Mine Area, northwest  
8 Queensland (P. A. P. a. G. Services, Trans.).

- 1 Ayan, T. (1965). *Chemical staining methods used in the identification of carbonate minerals*. Retrieved from  
2 [http://www.mta.gov.tr/v2.0/eng/dergi\\_pdf/65/11.pdf](http://www.mta.gov.tr/v2.0/eng/dergi_pdf/65/11.pdf).
- 3 Betts, P. G., Lister, G. S., & Pound, K. S. (1999). Architecture of a Palaeoproterozoic Rift System: Evidence from the Fiery Creek  
4 Dome region, Mt Isa terrane. *Australian Journal of Earth Sciences*, 46(4), 533-554. doi: 10.1046/j.1440-  
5 0952.1999.00721.x
- 6 Blenkinsop, T. G. (2012). Visualizing structural geology: From Excel to Google Earth. *Computers & Geosciences*, 45, 52-56. doi:  
7 10.1016/j.cageo.2012.03.007
- 8 Bureau of Mineral Resources (Cartographer). (1982). *Geology of the Lawn Hill Region*.
- 9 Carter, E. K., & Öpik, A. A. (Cartographer). (1961). *Lawn Hill 4-Mile Geological Map Sheet Series*.
- 0 Chen, X., & Chandra, N. (2004). The effect of heterogeneity on plane wave propagation through layered composites. *Composites*  
1 *Science and Technology*, 64(10–11), 1477-1493. doi: <http://dx.doi.org/10.1016/j.compscitech.2003.10.024>
- 2 Collins, G. S., Kenkmann, T., Osinski, G. R., & Wünnemann, K. (2008). Mid-sized complex crater formation in mixed  
3 crystalline-sedimentary targets: Insight from modeling and observation. *Meteoritics & Planetary Science*, 43(12), 1955-  
4 1977. doi: 10.1111/j.1945-5100.2008.tb00655.x
- 5 Collins, G. S., & Melosh, H. J. (2003). Acoustic fluidization and the extraordinary mobility of sturzstroms. *Journal of*  
6 *Geophysical Research*, 108(B10), 2473. doi: 10.1029/2003jb002465
- 7 de Keyser, F., & Cook, P. J. (1972). *Geology of the middle Cambrian phosphorites and associated sediments of northwestern*  
8 *Queensland*. (Bulletin 138). Canberra: Australian Government Publishing Service.
- 9 Denaro, T. J., Culpeper, L. G., Morwood, D. A., & Burrows, P. E. (1999). *Mines and mineralisation of the Lawn Hill 1:250 000*  
0 *Sheet area, north-west Queensland*. (23393).
- 1 Dence, M. R. (2002). Re-examining Structural Data from Impact Craters on the Canadian Shield in the Light of Theoretical  
2 Models. In J. Plado & L. Pesonen (Eds.), *Impacts in Precambrian Shields* (pp. 59-79): Springer Berlin Heidelberg.
- 3 Dietz, R. S. (1959). Shatter Cones in Cryptoexplosion Structures (Meteorite Impact?). *The Journal of Geology*, 67(5), 496-505.  
4 doi: 10.2307/30056104
- 5 Draper, J. (2007). Georgina basin—an early palaeozoic carbonate petroleum system in Queensland. *APPEA*, 47, 12.
- 6 Dypvik, H., Burchell, M., & Claeys, P. (2004). Impacts into Marine and Icy Environments — A Short Review. In H. Dypvik, M.  
7 Burchell & P. Claeys (Eds.), *Cratering in Marine Environments and on Ice* (pp. 1-20): Springer Berlin Heidelberg.
- 8 Feltrin, L. (2006). *Probabilistic and deterministic models of Pb-Zn mineralisation and post-mineralisation megabreccia in the*  
9 *Lawn Hill region, Australia*. (PhD), James Cook University, Townsville, Qld., Retrieved from  
0 <http://eprints.jcu.edu.au/1614/>
- 1 Feltrin, L., Oliver, N. H. S., Kelso, I. J., & King, S. (2003). Basement metal scavenging during basin evolution: Cambrian and  
2 Proterozoic interaction at the Century ZnPbAg Deposit, Northern Australia. *Journal of Geochemical Exploration*, 78-  
3 79(0), 159-162. doi: 10.1016/s0375-6742(03)00127-4
- 4 Feltrin, L., & Oliver, N. S. (2014). Timing and origin of megabreccia and folds along the Early Middle Cambrian margin of the  
5 Georgina Basin, Australia. *Carbonates and Evaporites*, 29(1), 3-31. doi: 10.1007/s13146-014-0193-6
- 6 Ferguson, C. L., & Phillips, D. (2001). <sup>40</sup>Ar/<sup>39</sup>Ar and K-Ar age constraints on the timing of regional deformation, south coast of  
7 New South Wales, Lachlan Fold Belt: problems and implications. *Australian Journal of Earth Sciences*, 48, 395-408.
- 8 French, B. M. (1998). *Traces of catastrophe: A handbook of shock-metamorphic effects in terrestrial meteorite impact structures*.  
9 Houston: Lunar and Planetary Institute.
- 0 Geological Survey of Queensland. (2011). *North-West Queensland Mineral and Energy Province Report*. Brisbane: Kingswood  
1 Press.
- 2 Grieve, R. A. F., & Masaitis, V. L. (1994). The Economic Potential of Terrestrial Impact Craters. *International Geology Review*,  
3 36(2), 105-151. doi: 10.1080/00206819409465452
- 4 Grieve, R. A. F., & Theriault, A. M. (2004). Observations at terrestrial impact structures: Their utility in constraining crater  
5 formation. *Meteoritics and Planetary Science*, 39(2), 199-216.
- 6 Haines, P. W. (2005). Impact cratering and distal ejecta: the Australian record. *Australian Journal of Earth Sciences*, 52(4-5),  
7 481-507. doi: 10.1080/08120090500170351
- 8 Haines, P. W., Hand, M., & Sandiford, M. (2001). Palaeozoic synorogenic sedimentation in central and northern Australia: A  
9 review of distribution and timing with implications for the evolution of intracontinental orogens. *Australian Journal of*  
0 *Earth Sciences*, 48(6), 911-928. doi: 10.1046/j.1440-0952.2001.00909.x
- 1 Hughes, D. W., & Williams, I. P. (2000). The velocity distributions of periodic comets and stream meteoroids. *Monthly Notices of*  
2 *the Royal Astronomical Society*, 315(3), 629-634. doi: 10.1046/j.1365-8711.2000.03435.x
- 3 Huson, S., Pope, M., Watkinson, A. J., & Foit, F. (2010). Deformational features and impact-generated breccia from the Sierra  
4 Madera impact structure, west Texas. *Geological Society of America Bulletin*, 123(1-2), 371-383. doi: 10.1130/b30183.1
- 5 Hutton, L. J. (1992). *Report on investigation of postulated astrobleme, Lawn Hill*. Australian Heritage Commission, Canberra.
- 6 Jiang, J., Gao, M. R., Qiu, Y. H., Wang, G. S., Liu, L., Cai, G. B., & Yu, S. H. (2011). Confined crystallization of polycrystalline  
7 high-magnesium calcite from compact Mg-ACC precursor tablets and its biological implications. *CrystEngComm*, 13(3),  
8 952. doi: 10.1039/c0ce00153h
- 9 Jourdan, F., Hodges, K., Sell, B., Schaltegger, U., Wingate, M. T. D., Evins, L. Z., Soderlund, U., Haines, P. W., Phillips, D., &  
0 Blenkinsop, T. (2014). High-precision dating of the Kalkarindji large igneous province, Australia, and synchrony with  
1 the Early-Middle Cambrian (Stage 4-5) extinction. *Geology*, 42(6), 543-546. doi: 10.1130/g35434.1
- 2 Kenkmann, T., Reimold, W. U., Khirfan, M., Salameh, E., Khoury, H., & Konsul, K. (2010). The complex impact crater Jebel  
3 Waqf as Suwwan in Jordan: Effects of target heterogeneity and impact obliquity on central uplift formation. *Geological*  
4 *Society of America Special Papers*, 465, 471-487. doi: 10.1130/2010.2465(23)
- 5 Kenkmann, T., Wittmann, A., & Scherler, D. (2004). Structure and impact indicators of the Cretaceous sequence of the ICDP drill  
6 core Yaxcopoil-1, Chicxulub impact crater, Mexico. *Meteoritics & Planetary Science*, 39(7), 1069-1088. doi:  
7 10.1111/j.1945-5100.2004.tb01129.x

- 1 Kieffer, S. W. (1971). Shock metamorphism of the Coconino Sandstone at Meteor Crater, Arizona. *Journal of Geophysical*  
2 *Research*, 76(23), 5449-5473. doi: 10.1029/JB076i023p05449
- 3 Kieffer, S. W., Phakey, P. P., & Christie, J. M. (1976). Shock processes in porous quartzite: Transmission electron microscope  
4 observations and theory. *Contributions to Mineralogy and Petrology*, 59(1), 41-93. doi: 10.1007/bf00375110
- 5 Kruse, P. D., Dunster, J. N., & Munson, T. (2013). Chapter 28: Georgina Basin. In M. Ahmad & T. J. Munson (Eds.), *Geology*  
6 *and mineral resources of the Northern Territory* (Vol. Special Publication 5., pp. 57): Northern Territory Geological  
7 Survey.
- 8 Langford, R. P., Wilford, G. E., Truswell, E. M., & Isern, A. R. (1988). Palaeogeographic atlas of Australia *Palaeogeographic*  
9 *atlas of Australia* (Vol. 10, pp. 37). Canberra: Australian Geological Survey Organisation.
- 0 Lindsay, J., & Brasier, M. (2006). Impact craters as biospheric microenvironments, Lawn Hill Structure, Northern Australia.  
1 *Astrobiology*, 6(2), 348-363. doi: 10.1089/ast.2006.6.348
- 2 Lisle, R. J. (1985). The use of the orientation tensor for the description and statistical testing of fabrics. *Journal of Structural*  
3 *Geology*, 7(1), 115-117. doi: 10.1016/0191-8141(85)90119-1
- 4 Lugli, S., Reimold, W., & Koeberl, C. (2005). Silicified Cone-in-Cone Structures from Erfoud (Morocco): A Comparison with  
5 Impact-Generated Shatter Cones. In C. Koeberl & H. Henkel (Eds.), *Impact Tectonics* (pp. 81-110): Springer Berlin  
6 Heidelberg.
- 7 Macke, R. J., Britt, D. T., Kiefer, W. S., Irving, A. J., & Consolmagno, G. J. (2011). *Porosity, magnetic susceptibility, and density*  
8 *of lunar meteorites*. Paper presented at the 74th Annual Meeting of the Meteoritical Society, London, U.K.  
9 <http://dx.doi.org/10.1111/j.1945-5100.2011.01221.x>
- 0 Manton, W. I. (1965). The orientation and origin of shatter cones in the Vredefort ring. *Annals of the New York Academy of*  
1 *Sciences*, 123(2), 1017-1048. doi: 10.1111/j.1749-6632.1965.tb20415.x
- 2 Megirian, D. (1992). Interpretation of the Miocene Carl Creek limestone, northwestern Queensland. *Beagle: Records of the*  
3 *Museums and Art Galleries of the Northern Territory*, The, 9, 219-248.
- 4 Meinhold, G., Arslan, A., Lehnert, O., & Stampfli, G. M. (2011). Global mass wasting during the Middle Ordovician: Meteoritic  
5 trigger or plate-tectonic environment? *Gondwana Research*, 19(2), 535-541. doi:  
6 <http://dx.doi.org/10.1016/j.gr.2010.07.001>
- 7 Melosh, H. J. (1989). *Impact cratering : a geologic process*. New York Oxford: Oxford University Press ;Clarendon Press.
- 8 Miljkovic, K., Collins, G. S., Chapman, D. J., Patel, M. R., & Proud, W. G. (2012). *High-velocity impacts in porous solar system*  
9 *materials*. <http://dx.doi.org/10.1063/1.3686416>
- 0 Moore, C. H. (2001). Chapter 3 The Nature and Classification of Carbonate Porosity. In C. H. Moore (Ed.), *Developments in*  
1 *Sedimentology* (Vol. Volume 55, pp. 37-60): Elsevier.
- 2 Munson, T. J., Ahmad, M., & Dunster, J. N. (2013). Chapter 39: Carpentaria Basin. In M. Ahmad & T. J. Munson (Eds.),  
3 *Northern Territory Geological Survey Special Publication 5* (pp. 1-18). Darwin.
- 4 Northern Territory Geological Survey DME. (2011). NT Geological Regions 2500K. Retrieved 3 March, 2014, from  
5 [http://geoscience.nt.gov.au/GeosambaU/strike\\_gs\\_webclient/default.aspx](http://geoscience.nt.gov.au/GeosambaU/strike_gs_webclient/default.aspx)
- 6 Opik, A. A., Carter, E. K., & Randal, M. A. (1961). *Notes on the first edition Camooweal geological sheet, Queensland.*  
7 (1973/83). Canberra: Bureau of Mineral Resources, Geology and Geophysics.
- 8 Ormö, J., Lindström, M., Lepinette, A., Martinez-Frias, J., & Diaz-Martinez, E. (2006). Cratering and modification of wet-target  
9 craters: Projectile impact experiments and field observations of the Lockne marine-target crater (Sweden). *Meteoritics &*  
0 *Planetary Science*, 41(10), 1605-1612. doi: 10.1111/j.1945-5100.2006.tb00438.x
- 1 Ormö, J., Sturkell, E., Alwmark, C., & Melosh, J. (2014). First known Terrestrial Impact of a Binary Asteroid from a Main Belt  
2 Breakup Event. *Sci. Rep.*, 4. doi: 10.1038/srep06724
- 3 Osinski, G. R., Spray, J. G., & Grieve, R. A. F. (2008). Impact melting in sedimentary target rocks: An assessment. *Geological*  
4 *Society of America Special Papers*, 437, 1-18. doi: 10.1130/2008.2437(01)
- 5 Phillips, D., & Harris, J. W. (2008). Provenance studies from <sup>40</sup>Ar/<sup>39</sup>Ar dating of mineral inclusions in diamonds: Methodological  
6 tests on the Orapa kimberlite, Botswana. *Earth and Planetary Science Letters*, 274.
- 7 Phillips, D., Harris, J. W., & Kiviets, G. B. (2004). <sup>40</sup>Ar/<sup>39</sup>Ar analyses of clinopyroxene inclusions in African diamonds:  
8 implications for source ages of detrital diamonds. *Geochimica et Cosmochimica Acta*, 68(151-168).
- 9 Pilkington, M., & Grieve, R. A. F. (1992). The geophysical signature of terrestrial impact craters. *Reviews of Geophysics*, 30(2),  
0 161. doi: 10.1029/92rg00192
- 1 Portenga, E. W., & Bierman, P. R. (2011). Understanding Earth's eroding surface with <sup>10</sup>Be. *GSA Today*, 21(8), 4-10. doi:  
2 10.1130/G111A.1
- 3 Pouchou, J. L., & Pichoir, F. (1984). New model for quantitative x-ray microanalysis. Part i: Application to the analysis of  
4 homogeneous samples. *Recherche Aerospatiale (English Edition)*(3), 13-38.
- 5 Rager, A. H., Smith, E. I., Scheu, B., & Dingwell, D. B. (2014). The effects of water vaporization on rock fragmentation during  
6 rapid decompression: Implications for the formation of fluidized ejecta on Mars. *Earth and Planetary Science Letters*,  
7 385, 68-78. doi: 10.1016/j.epsl.2013.10.029
- 8 Rands, W. H. (1901). *GSQ publication 159 Annual progress report for the year 1900.* (55315).
- 9 Reimold, W. U., Koeberl, C., & Gibson, R. L. (2005). Economic Mineral Deposits in Impact Structures: A Review (pp. 479-552).  
0 Berlin, Heidelberg: Springer Berlin Heidelberg.
- 1 Renne, P. R., Cassata, W. S., & Morgan, L. E. (2009). The isotopic composition of atmospheric argon and <sup>40</sup>Ar/<sup>39</sup>Ar  
2 geochronology: Time for a change? *Quaternary Geochronology*, 4(4), 288-298. doi:  
3 <http://dx.doi.org/10.1016/j.quageo.2009.02.015>
- 4 Renne, P. R., Swisher, C. C., Karner, A. L., Owens, D. B., & DePaolo, D. J. (1998). Intercalibration of standards, absolute ages  
5 and uncertainties in <sup>40</sup>Ar/<sup>39</sup>Ar dating. *Chemical Geology*, 145, 117-152.
- 6 Salameh, E., Khoury, H., Reimold, W. U., & Schneider, W. (2008). The first large meteorite impact structure discovered in the  
7 Middle East: Jebel Waqf as Suwwan, Jordan. *Meteoritics and Planetary Science*, 43(10), 1681-1690.

- 1 Salisbury, J. A., Tomkins, A. G., & Schaefer, B. F. (2008). New insights into the size and timing of the Lawn Hill impact  
2 structure: relationship to the Century Zn – Pb deposit. *Australian Journal of Earth Sciences*, 55(4), 587-603.
- 3 Schmieder, M., Schwarz, W. H., Trieloff, M., Tohver, E., Buchner, E., Hopp, J., & Osinski, G. R. (2015). New <sup>40</sup>Ar/<sup>39</sup>Ar dating  
4 of the Clearwater Lake impact structures (Québec, Canada) – Not the binary asteroid impact it seems? *Geochimica et*  
5 *Cosmochimica Acta*, 148(0), 304-324. doi: <http://dx.doi.org/10.1016/j.gca.2014.09.037>
- 6 Schmitz, B., Tassinari, M., & Peucker-Ehrenbrink, B. (2001). A rain of ordinary chondritic meteorites in the early Ordovician.  
7 *Earth and Planetary Science Letters*, 194(1–2), 1-15. doi: [http://dx.doi.org/10.1016/S0012-821X\(01\)00559-3](http://dx.doi.org/10.1016/S0012-821X(01)00559-3)
- 8 Sellés-Martínez, J. (1996). Concretion morphology, classification and genesis. *Earth-Science Reviews*, 41(3-4), 177-210. doi:  
9 10.1016/s0012-8252(96)00022-0
- 0 Senft, L. E., & Stewart, S. T. (2007). Modeling impact cratering in layered surfaces. *Journal of Geophysical Research: Planets*,  
1 112(E11), E11002. doi: 10.1029/2007JE002894
- 2 Sharp, Z. D., Essene, E. J., & Smyth, J. R. (1992). Ultra-high temperatures from oxygen isotope thermometry of a coesite-sanidine  
3 grosspyrite. *Contributions to Mineralogy and Petrology*, 112(2-3), 358-370. doi: 10.1007/BF00310466
- 4 Shoemaker, E. M., & Kieffer, S. W. (1974). Guidebook to the geology of Meteor Crater, Arizona. (pp. 66). Tempe, Arizona:  
5 Center for Meteorite Studies, Arizona State University.
- 6 Shoemaker, E. M., & Shoemaker, C. S. (1990). Proterozoic Impact Record of Australia. *LPI Contributions*, 746, 2.
- 7 Shoemaker, E. M., & Shoemaker, C. S. (1996). The Proterozoic impact record of Australia. *AGSO Journal of Australian Geology*  
8 *& Geophysics*, 16, 379-398.
- 9 Smart, J., Grimes, K. G., Douth, H. F., & Pinchin, J. (1980). *The Mesozoic Carpentaria Basin and the Cainozoic Karumba*  
0 *Basin, North Queensland*. Canberra: Bureau of mineral Resources, Geology and Geophysics.
- 1 Smith, A. G. (1999). Gondwana: Its shape, size and position from Cambrian to Triassic times. *Journal of African Earth Sciences*,  
2 28(1), 71-97. doi: [http://dx.doi.org/10.1016/S0899-5362\(99\)00020-2](http://dx.doi.org/10.1016/S0899-5362(99)00020-2)
- 3 Smith, K. G. (1967). *The geology of the Georgina Basin*. (1967/60). Commonwealth of Australia.
- 4 Smith, K. G. (1972). *The stratigraphy of the Georgina Basin*. Canberra: Australian Govt. Publishers.
- 5 Solem, J. C. (1994). Density and size of comet Shoemaker-Levy 9 deduced from a tidal breakup model. *Nature*, 370(6488), 349-  
6 351.
- 7 Southgate, P. N. (1986). The Gowers Formation and Bronco Stromatolith Bed, two new stratigraphic units in the Undilla portion  
8 of the Georgina Basin. *Queensland Government Mining Journal*, 87(1019), 4.
- 9 Spray, J. G., Butler, H. R., & Thompson, L. M. (2004). Tectonic influences on the morphometry of the Sudbury impact structure:  
0 Implications for terrestrial cratering and modeling. *Meteoritics & Planetary Science*, 39(2), 287-301. doi:  
1 10.1111/j.1945-5100.2004.tb00341.x
- 2 State of Queensland DNRM. (2011a). GSQ detailed geology structures - Lawn Hill. Retrieved 3 March, 2014, from  
3 <https://webgis.dme.qld.gov.au/webgis/webqmin/viewer.htm>
- 4 State of Queensland DNRM. (2011b). Rock Unit Surface - Lawn Hill. Retrieved 3 Mar, 2014, from  
5 <https://webgis.dme.qld.gov.au/webgis/webqmin/viewer.htm>
- 6 Steiger, R. H., & Jager, E. (1977). Subcommission on geochronology: convention on the use of decay constants in ger- and  
7 cosmochronology. *Earth and Planetary Science*, 36, 359-362.
- 8 Stewart, A., & Mitchell, K. (1987). Shatter cones at the Lawn Hill circular structure, northwestern Queensland: presumed  
9 astrobleme. *Australian Journal of Earth Sciences*, 34(4), 477-485. doi: 10.1080/08120098708729427
- 0 Sturkell, E., & Ormo, J. (1997). Impact-related clastic injections in the marine Ordovician Lockne impact structure, Central  
1 Sweden. *Sedimentology*, 44(5), 793-804. doi: 10.1046/j.1365-3091.1997.d01-54.x
- 2 Sweet, I. P., & Hutton, L. J. (1980). *The geology of the Lawn Hill/Riversleigh region, Queensland*. (1980/43 c.3). Canberra,  
3 Australia: Bureau of Mineral Resources Geology and Geophysics.
- 4 Szulc, S. A. (1992). *The stratigraphic reconstruction of a mega-breccia : a sedimentological study of the south western corner of*  
5 *the Lawn Hill Outlier*. (B Sc (Hons)), James Cook University, Townsville, Qld.,.
- 6 Tewksbury, B. J., Dokmak, A. A. K., Tarabees, E. A., & Mansour, A. S. (2012). Google Earth and geologic research in remote  
7 regions of the developing world: An example from the Western Desert of Egypt. *Geological Society of America Special*  
8 *Papers*, 492, 23-36. doi: 10.1130/2012.2492(02)
- 9 Thiot, J. F., & Pouchou, J. L. (Eds.). (1996). *EPMA quantitative X-ray mapping*: San Francisco Press.
- 0 Tucker, D. H., Wyatt, B. W., Druce, E. C., Mathur, S. P., & Harrison, P. L. (1979). The upper crustal geology of the Georgina  
1 Basin region. *BMR Journal of Australian Geology and Geophysics*, 4(3), 209-226.
- 2 Vollmer, F. W. (1990). An application of eigenvalue methods to structural domain analysis. *Geological Society of America*  
3 *Bulletin*, 102(6), 786-791. doi: 10.1130/0016-7606(1990)102<0786:aaemt>2.3.co;2
- 4 Walter, M. R. (1972). Stromatolites and biostratigraphy of the Australian Precambrian and Cambrian. *Special papers in*  
5 *palaeontology*, 11, 190.
- 6 Wang, G., Zhang, S., Yu, M., Li, H., & Kong, Y. (2014). Investigation of the shock wave propagation characteristics and  
7 cavitation effects of underwater explosion near boundaries. *Applied Ocean Research*, 46(0), 40-53. doi:  
8 <http://dx.doi.org/10.1016/j.apor.2014.02.003>
- 9 Wilson, I. H., & Hutton, L. J. (1980). Geological field work in Mount Isa district—August and September, 1980. *Geol. Survey*  
0 *Queensland Record*, 34, 12–18.
- 1 Wünnemann, K., Collins, G. S., & Melosh, H. J. (2006). A strain-based porosity model for use in hydrocode simulations of  
2 impacts and implications for transient crater growth in porous targets. *Icarus*, 180(2), 514-527. doi:  
3 10.1016/j.icarus.2005.10.013
- 4 Wünnemann, K., Collins, G. S., & Osinski, G. R. (2008). Numerical modelling of impact melt production in porous rocks. *Earth*  
5 *and Planetary Science Letters*, 269(3-4), 530-539. doi: 10.1016/j.epsl.2008.03.007
- 6 Zappalà, V., Cellino, A., Gladman, B. J., Manley, S., & Migliorini, F. (1998). Asteroid Showers on Earth after Family Breakup  
7 Events. *Icarus*, 134(1), 176-179. doi: <http://dx.doi.org/10.1006/icar.1998.5946>

1 Zhuang, S., Ravichandran, G., & Grady, D. E. (2003). An experimental investigation of shock wave propagation in periodically  
2 layered composites. *Journal of the Mechanics and Physics of Solids*, 51(2), 245-265. doi:  
3 [http://dx.doi.org/10.1016/S0022-5096\(02\)00100-X](http://dx.doi.org/10.1016/S0022-5096(02)00100-X)

4

5

## FIGURE CAPTIONS

Figure 1: Locality map showing the general location, rock units, and strips (NE and E) used to ground truth the virtual bedding interpretation (kmz file). A larger scale view of the E strip can be found in figure 5. The position of the Century Mine has been marked including the area previously mapped (Szulc, 1992). Sample locations of dolomite-chert breccias (LH-101 and -648) have been shown. The boundary of the Boodjamulla National Park lies ~15 km to the W of the LHS, and represents the closest outcrops of the Georgina Basin. The location of figure 6 is marked with the white rectangle. The white line marks the position of the section shown in figure 4. Supplementary material has been provided, in the form of a kmz file that opens in Google Earth, displaying additional photographs at the sample locations. The inset shows the location of the Georgina Basin, the Undilla Sub-basin and the Mt Isa Inlier relative to the LHS and Mt Isa. The lithological legend used in figure 1 is the same for all other figures.

Figure 2: Detailed geological map of the Gum Hole Plain. The sample locations of the melt rocks and shatter cones (shown in figures 10 and 11), and the dolomite-chert breccia (LH-183) have been included. The area where loose rubble with the shatter cones were found is displayed, including the area mapped by Stewart and Mitchell (1987). The position of in situ shatter cones is marked with solid lines, and the estimated region of melt with a dashed circle. The sample locations for  $^{40}\text{Ar}$ - $^{39}\text{Ar}$  dating are indicated (JS-006/LH-355 and JS-023). The exposed Mesoproterozoic rocks of the Lawn Hill Formation are shown, including the basal carbonaceous shale. The shale boundary was taken from the earlier mapping undertaken by Shoemaker and Shoemaker (1996). The breccia ringing the outer edge of the Gum Hole Plain is sandstone-quartz in a siliceous matrix. This type of breccia is also found between sandstone beds at Mt Jennifer. The legend to this figure is presented in figure 1.

Figure 3: A stratigraphic column for the LHS showing the Lawn Hill Formation and overlying sediments at the base of the Georgina Basin sequence. Jurassic (Gilbert River Formation and Mullaman beds) and Cenozoic sediments (Armraynald beds) unconformably covered rocks of the Georgina Basin sequence.

Figure 4: A cross section through the impact structure from SW to NE (section line shown in figure 1). The deformation of the Mesoproterozoic rocks of the Lawn Hill Formation in the Gum Hole Plain is consistent with regional deformation. Thin Cenozoic Armraynald beds cover the majority of the Gum Hole Plain rocks (Fig. 2). Shock heating and deformation appear to have affected the rocks in the impact centre to a maximum depth of ~160 to 170 m. (Salisbury et al., 2008).

Figure 5: Detailed map of the E strip (Fig. 1). Selected bedding measurements, illustrating the local deformation patterns, are shown. Overturning is more common in the inner region – see stereonet in figure 5b. The inset (figure 5c) shows the bedding surfaces (rectangles) with the associated younging directions (arrows) superimposed on the Google Earth topography with disks marking localities of breccia. Analyses of the sub-divided bedding data i.e. inner and outer sections do not reveal a preferred bedding orientation. The stereoplots in figures 5b and 5d are equal area, lower hemisphere plots of poles to bedding. The legend for figure 5a is presented in figure 1.

Figure 6: A detailed interpretation of bedding trends (yellow) and fault lines (red) within the NE strip using Google Earth base imagery. The deformation pattern shown is representative of the deformation within the dolomite. The majority of the folding occurred prior to fracturing, which led to the formation of the mega-breccia. Minor rotation of breccia blocks, post fracturing, is evident. The mega-clasts have no systematic orientation with fracturing occurring at 30 to 100 m scale. The location of figure 6 is shown with a white rectangle in figure 1.

Figure 7. Equal area, lower hemisphere stereoplots of poles to bedding within dolomite blocks of the main annulus, a) and b) show data for the NE and E strips respectively, c) shows the measurements collected by (Szulc, 1992) from a small region on the outer SW edge of the annulus. Bedding dips are mostly gentle-moderate with no preferred azimuthal orientation. The identifiable overturned bedding in the SW is more steeply dipping than the NE and E strips noting that the Szulc (1992) data did not differentiate between upright and overturned bedding planes. The poles to bedding within the NE strip cluster around the vertical. The abundance of stromatolite beds in the E strip enabled the determination of way-up criteria for a larger number of bedding planes.

Figure 8. Point, girdle and random distribution indices for the orientations of bedding (cf. Bureau of Mineral Resources, 1982; Vollmer, 1990) with contours of intensity drawn after Lisle (1985). Aggregate values for the NE and E strips, and SW domain correspond to the plots in figures 7a-c. Patterns for all data sets are generally intermediate between point and random distributions. Inner, middle and outer subdivision of NE and E data sets were used to identify any radial distinctive deformation and to identify the geographical equivalence between the smaller Szulc (1992) results and the full extent field data of this study. Similarity between NE strip middle and SW domain suggests that these localities may occupy comparable positions relative to the impact.

Figure 9: Geological maps of a) Mt Jennifer and b) Southern Outcrops (Bureau of Mineral Resources, 1982; State of Queensland DNRM, 2011b). Selected field data has been added to the base data to show bedding trends. Equal area, lower hemisphere stereoplots (insets to figures 9a and 9b) of poles to the dolomite/sandstone bedding within the particular large scale areas display the variation in bedding dip and orientation. The dolomite at the N end of Mt Jennifer and the Outer outcrop is sub-horizontal. The dolomite-chert breccia at Mt Jennifer shows dyke-like properties compared with the Mt Jennifer siliceous breccia, which is aligned with the local bedding (Fig. 12d). Monomict breccia was found along the contact between the dolomite and siliceous breccia unit at Mt Jennifer (Figs 13b and c). The legend to this figure is presented in figure 1.

Figure 10: Examples of melt rocks (a-c) that display the range of metamorphic effects found in the siltstone and sandstone rocks exposed in the centre of the Gum Hole Plain. The samples shown are located ~100 m from each other with a) LH-143 occurring at 18°41'32.27"S, 138°39'8.02"E; b) LH-145 at 18°41'32.76"S, 138°39'7.84"E; and c) LH-138 at 18°41'29.80"S, 138°39'5.08"E (Fig. 2).

Figure 11. Examples of shatter cones found in float on the surface of the Gum Hole Plain (Fig. 2). a) a loose cobble found close to LH-125 (18°41'26.57"S, 138°38'59.15"E); b) from a region of high abundance on the NE side of the mapped shatter cone area (LH-128 at 18°40'46.00"S, 138°39'31.20"E). Both samples show a change in the direction of the apices of the cones on the differing surfaces. The back surface of sample (b) is not shown but preserves apex orientations opposite to the displayed surface.

1  
2 *Figure 12. Dolomite-chert breccia is found within the deformed dolomite annulus surrounding the Gum Hole Plain (a – c) at the LHis*  
3 *including the inner southern outcrop. a) LH-648; b) LH-101 (Fig. 1); c) A large clast (~50 x 50 cm) of Thornton Limestone with fine chert*  
4 *banding. This sample is located at LH-620 (Fig. 1). A photograph showing the entire clast can be found in the Supplementary File, at LHis.kmz*  
5 */Annulus Breccias, LH-620. d) Breccia within dolomite at Mt Jennifer, which is compositionally similar to the other breccias except that the*  
6 *ratio of matrix vs clasts varies. The Mt Jennifer dykes are the only breccia that contains material from a lithology other than dolomite (see*  
7 *Supplementary File, LHis.kmz/Mt Jennifer and the Southern Outcrops: LH2-786), i.e. sandstone clasts that may have originated from the*  
8 *Widdallion Sandstone.*

9 *Figure 13. Examples of breccia types found in the LHis. a) Within the Gum Hole Plain, a re-brecciated dolomite breccia, LH-183 (Fig. 2).*  
0 *This material is clast dominant with clasts showing a history of fracturing. b) Mt Jennifer hosts a polymict breccia that contains fragments of*  
1 *Widdallion Sandstone located below the dolomite. c) Siliceous breccia identified as 'Border Waterhole Formation'. This image shows a breccia*  
2 *sill injected between layers of sandstone, and suggests the siliceous breccia may have originally been Widdallion Sandstone altered by the*  
3 *impact event. The siliceous breccia lining the inner edge of the dolomite annulus may also have originated from Widdallion Sandstone.*

4 *Figure 14. Sample JS-006 (LH-355) (Location: 18°40'58.31"S, 138°39'6.47"E) used for <sup>40</sup>Ar-<sup>39</sup>Ar dating. This PPL image shows the dark*  
5 *convoluted and contorted fluidal melt domain with the embedded siltstone breccia fragments (as labeled).*

6 *Figure 15. Sample JS-023 (Location: 18°41'31.89"S, 138°39'0.55"E) used for <sup>40</sup>Ar-<sup>39</sup>Ar dating. a) and b) are PPL and XPL images*  
7 *respectively of a single k-feldspar spherule. The scale is in mm.*

8 *Figure 16. Step heating diagrams used for <sup>40</sup>Ar-<sup>39</sup>Ar dating. Representative age spectra of the two samples analyzed. a) JS-006: a fluidal*  
9 *melt domain found in the central drill core LH-355. b) JS-023, which is located within float material (Fig. 2; LHis.kmz/Geochronology). Details*  
0 *of the analyses are presented in Table 1.*

1 *Table 1: Detailed geochronology results for the two samples selected from within the rocks at the LHis.*

## 2 *Supplementary Material*

3 *Tables S1-S3 Microprobe, XRD and XRF analyses for dolomite-chert breccia found within the deformed dolomite annulus.*

4 *Table S4. Microprobe analyses for impact melt particles and K-feldspar spherules from JS006*

5 *Table S5: Microprobe analyses of the dark, melt rich domains in a surface specimen, JS023, collected from close to the impact centre.*

6 *Supplementary File, LHis.kmz: This file displays additional photographs and supporting material. This file needs to be opened in Google*  
7 *Earth where all material is placed on the relevant geographical location.*

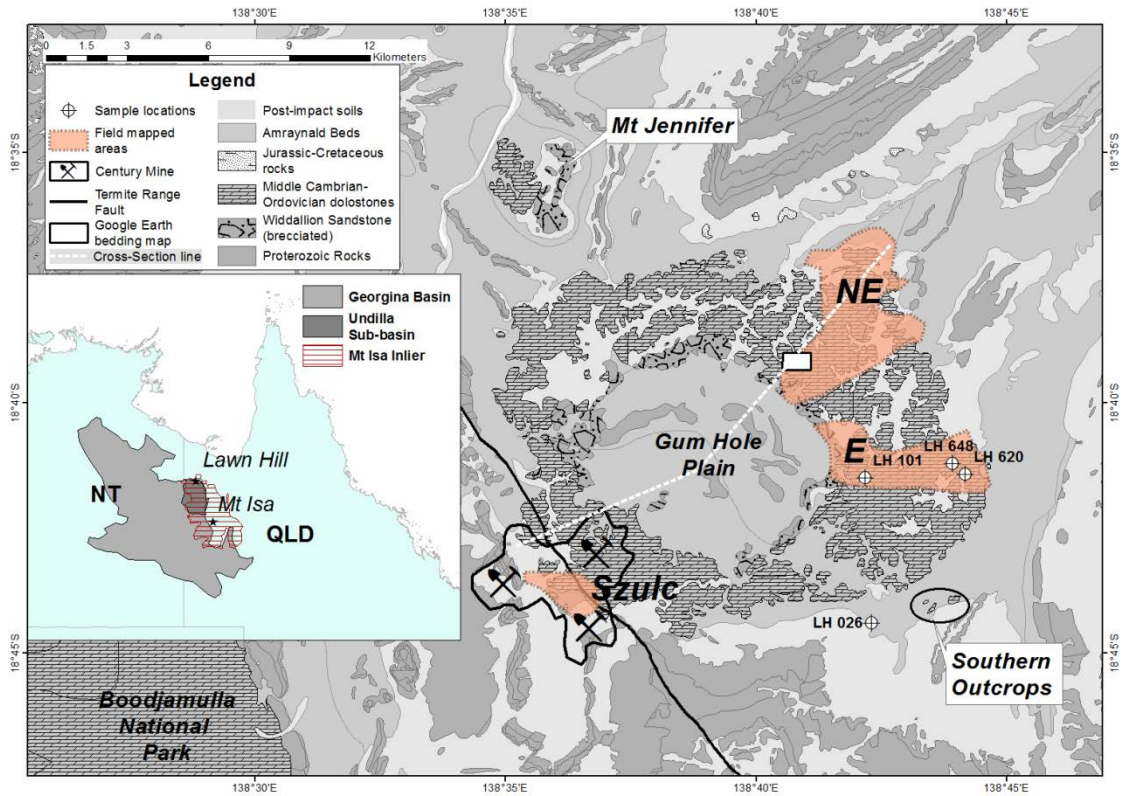


Figure 1: A locality Map showing the general location, rock units, and strips (NE & E) used to ground truth the virtual bedding interpretation (kmz file). A larger scale view of the east strip can be found at Fig. 16. The Century Mine Site boundary has been marked including the area previously mapped (Szulc, 1992) but now excavated. Sample location of the dolomite-chert breccias described (pins: LH101 and 648) have been included. Boodjamulla National Park lies less than 15 km to the west of the LHIS, the closest section of Georgina Basin to the outlier. Generally unbroken concretions are found at LH026 (18°44'24.30"S, 138°42'18.24"E), as well as on the surface of Gum Hole Plain but the concretions found within the Gum Hole Plain are predominantly fractured. The location of the Google Earth based bedding map (Fig. 4) is marked as a small white rectangle. White line shows position of section in Fig. 3. Supplementary material has been provided in the form of a kmz file using Google Earth software as a base map that displays additional photographs at the sample locations. The inset shows the location of the Georgina Basin, the Undilla Sub-basin and the Mt Isa Inlier as well as regional positioning of the LHIS and Mt Isa. The lithological legend is used for all of the maps presented.

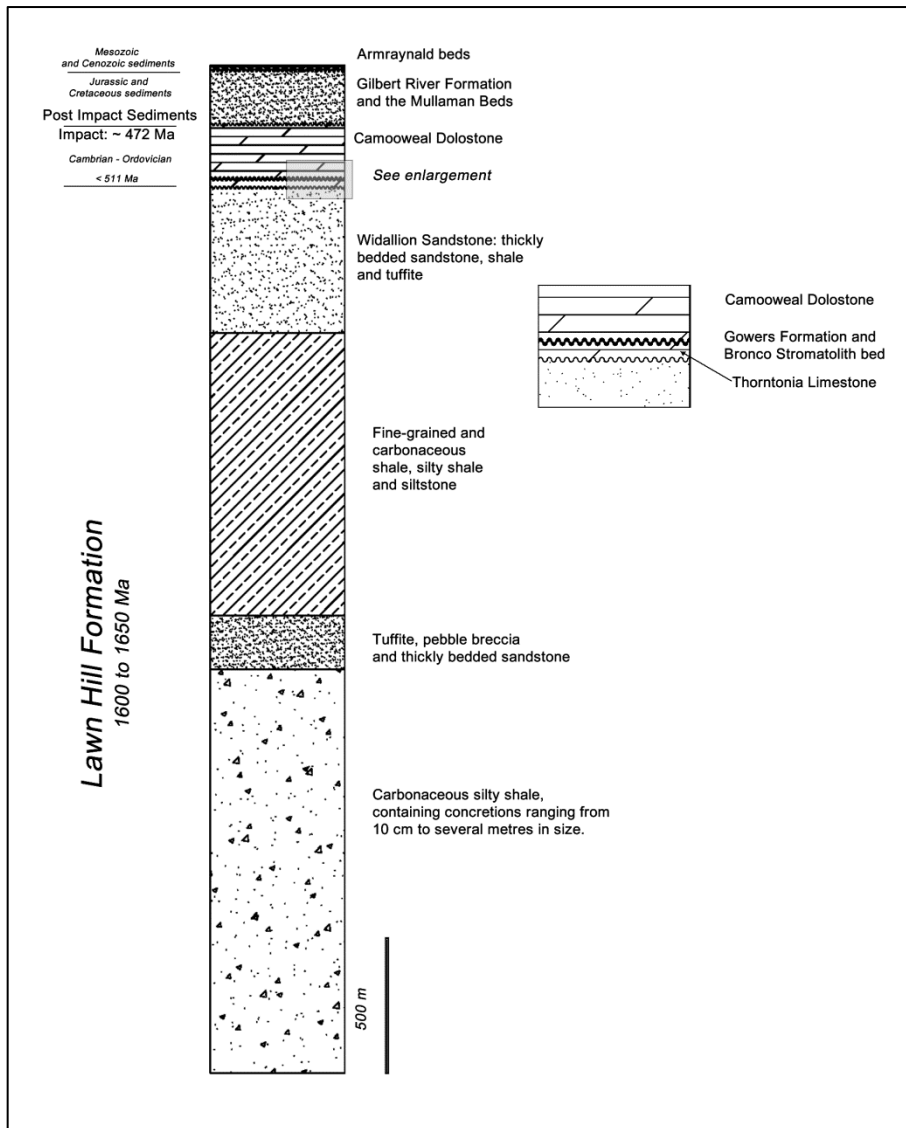


Figure 2: The stratigraphic column of the Lawn Hill impact site showing the Lawn Hill Formation members and younger sediments. The impact occurred at  $472 \pm 8$  Ma indicating the target surface was most likely the Camooweal Dolostone rather than the hypothesized (Salisbury et al., 2008) Thornton Limestone. The presence of the thin layer of LH stromatolites, assumed to be evidence of the Bronco Stromatolith beds, with overlying dolomite throughout the E strip supports the  $^{40}\text{Ar}$ - $^{39}\text{Ar}$  age presented. The Jurassic (Gilbert River Formation and Mullaman beds) sedimentation coupled with Cenozoic sedimentation (Armraynald beds) provided post-impact protection to the impact features including the shatter cones, melt rocks and dolomite annulus formed in the Mid-Ordovician. Erosional processes have removed any evidence of the Jurassic rocks overlying the dolomite. The shatter cone cobbles found on the surface of the Gum Hole Plain may have been brought upward by the "floating" abilities of the Armraynald beds.

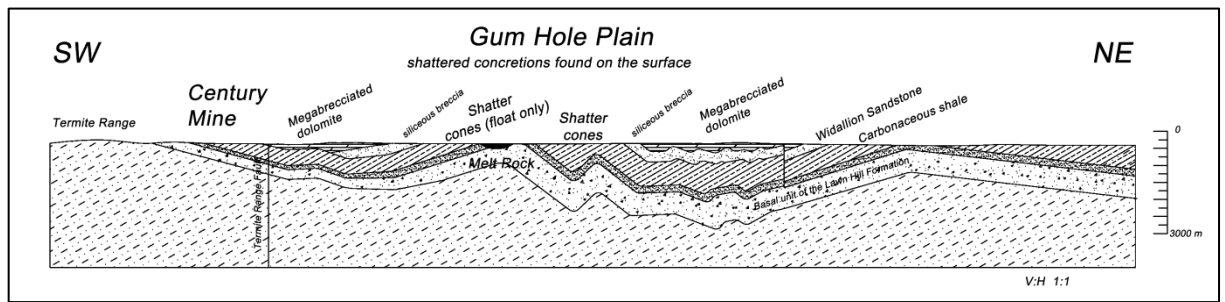


Figure 3: A cross section through the impact structure from SW to NE across line shown in Fig 1. The deformation of the Mesoproterozoic rocks of the Lawn Hill Formation in the Gum Hole Plain is consistent with regional deformation, the result of the Isan Orogeny (1590 to 1500 Ma). Thin Cenozoic Armraynald beds cover the majority of the Gum Hole Plain rocks (see Fig. 8). Shock heating and deformation appear to have affected the rocks in the impact centre to a maximum depth of ~ 160 to 170 m. (Salisbury et al., 2008). The reflectance profile of LH355 showed a Ro % value anomaly (high) at 151 m located directly overlying a breccia, indicating temperatures exceeding 200 °C. This anomaly correlates with section of drill core LH355 above that examined by Salisbury et al. (2008), selected because of the presence of melt.

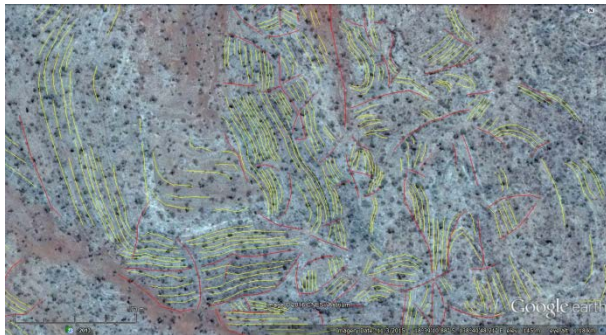


Figure 4. A detailed interpretation of bedding (yellow) and fracture/fault lines (red) within the NE strip using Google Earth base imagery, representative of the deformation within the dolomite. The majority of the folding occurred prior to the fracturing determined by the block boundaries. Minor rotation post fracturing is present. The megaclasts have no systematic orientation with fracturing occurring on the 30 to 100 m scale. Location of figure given by white rectangle in Fig. 1

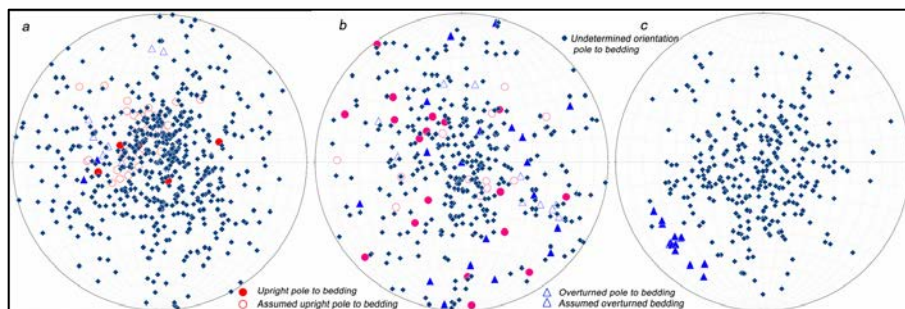


Figure 5. Equal area, lower hemisphere stereoplots of poles to the dolomite bedding within the main annulus, a) and b) are NE and E strips respectively, c) is measurements by (Szulc, 1992) from a small region on the outer SW region of the annulus. Bedding dips are mostly gentle-moderate with no preferred azimuthal orientation. The identifiable overturned bedding in the SW is more steeply dipping than the NE and E strips noting that the Szulc (1992) data did not indicate known upright bedding. Co-location of bedding to a known orientation was used to make the assumption of bedding orientation. The known/assumed upright pole to bedding within the NE strip appears to be clustered around the horizontal but trending towards the SE. The abundance of stromatolite beds in the E strip enabled a larger number of determinations of bedding way-up. This perhaps shows the clustering in a) and c) is artificial.

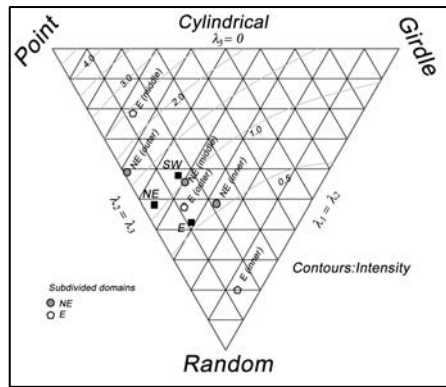


Figure 6. PGR indexes for the orientations of bedding (cf. Bureau of Mineral Resources, 1982; Vollmer, 1990). Contours of Intensity drawn after Lisle (1985). Aggregate values for NE and E strips, and SW domain correspond to plots in Fig. 8 a - c. Inner, middle and outer subdivision of NE and E data sets used to identify any radial distinctive deformation. Patterns are generally intermediate between point and random distributions. Similarity between NE strip middle and SW domain suggests that these localities may occupy comparable positions relative to the impact.

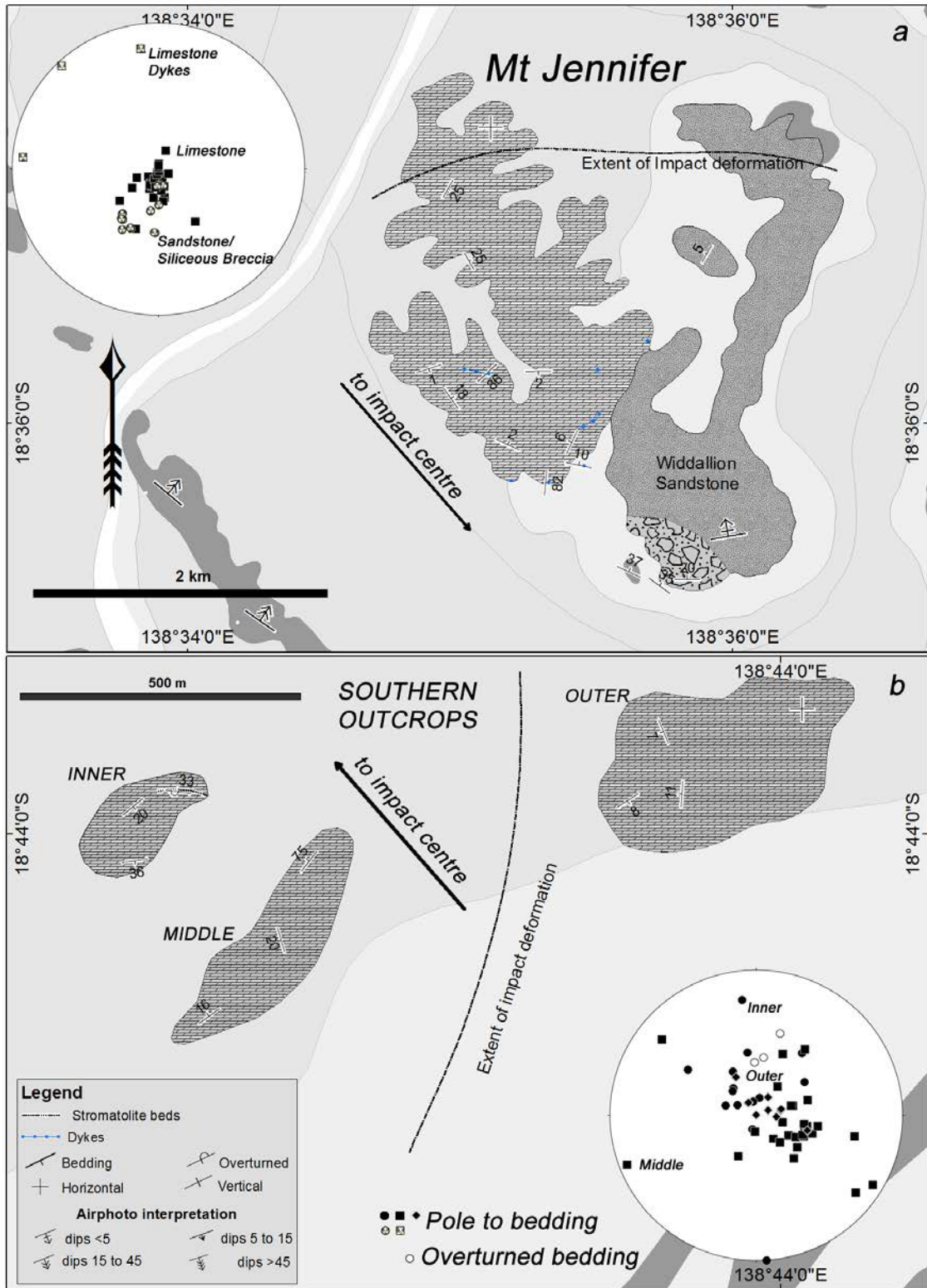


Figure 7: Maps of a) Mt Jennifer and b) Southern Outcrops (Bureau of Mineral Resources, 1982; State of Queensland DNRM, 2011). Selected field data has been added to the base data to show the bedding trends. Equal area, lower hemisphere stereoplots of poles to the dolomite/sandstone bedding within the particular large scale areas displays the variation in bedding dip and orientation. The dolomite at the northern end of Mt Jennifer and the Outer outcrop is sub-horizontal. The dolomite-chert breccia at Mt Jennifer shows dyke-like properties compared with the Mt Jennifer siliceous breccia which is aligned with the local bedding (see Fig. 11d this study). Autoclastic breccia was found along the contact between the dolomite and siliceous breccia unit at Mt Jennifer (see Fig. 12b & c).

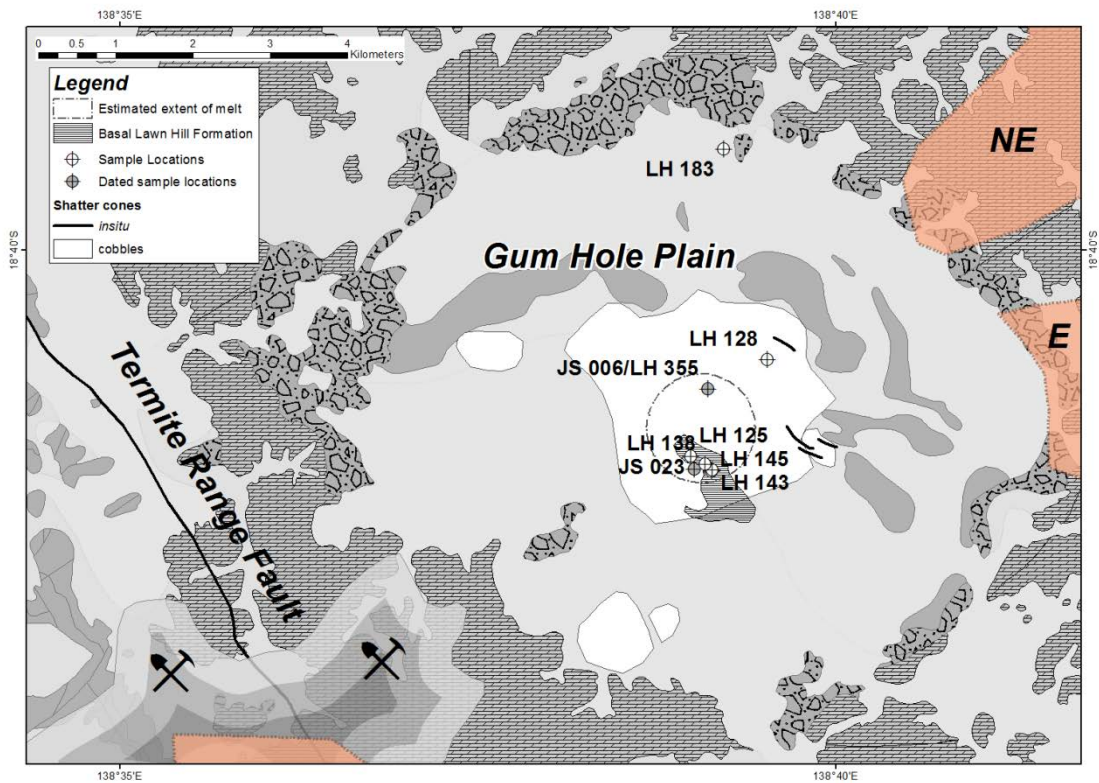


Figure 8: Detailed map of the Gum Hole Plain. Sample location of the melt rocks and shatter cones (shown in Fig. 9 & 10 respectively) and the dolomite-chert breccia (LH 183) found within the plain have been included. The area over which the shatter cone float were found is displayed, including that mapped by Stewart and Mitchell (1987). The *in situ* shatter cones are marked by solid lines. The location of the material used in the  $^{40}\text{Ar}$ - $^{39}\text{Ar}$  dating is marked (JS006/LH355 and JS023). The estimated region of melt is marked by a dashed circle. The exposed Mesoproterozoic rocks of the Lawn Hill Formation are shown, including the basal carbonaceous shale. The shale boundary was taken from the earlier mapping undertaken by Shoemaker and Shoemaker (1996). The presence of this basal unit at the surface is consistent with the projected cross-section. The breccia ringing the outer edge of the Gum Hole Plain is sandstone-quartz in a siliceous matrix. The clasts in the breccia are dominantly angular (90%) but the remaining 10% are markedly rounded. This texture was described as most likely generated during impact as fall-back breccias with clast rounding due to interaction with high-velocity gaseous ejection (Lindsay & Brasier, 2006). This breccia is also found between sandstone beds at Mt Jennifer.



Figure 9: These melt rocks (a-c) display the range of metamorphic effects found in the siltstone/sandstone rocks exposed in the centre of the Gum Hole Plain. The melt rock at surface covered an area 1 km in length but only ~ 150 m wide running NW-SE, originally mapped by Shoemaker and Shoemaker (1996) The samples shown are located ~100 m from each other specifically at a) LH143: 18°41'32.27"S, 138°39'8.02"E b) LH145: 18°41'32.76"S, 138°39'7.84"E and c) LH138: 18°41'29.80"S, 138°39'5.08"E (see Fig. 8).

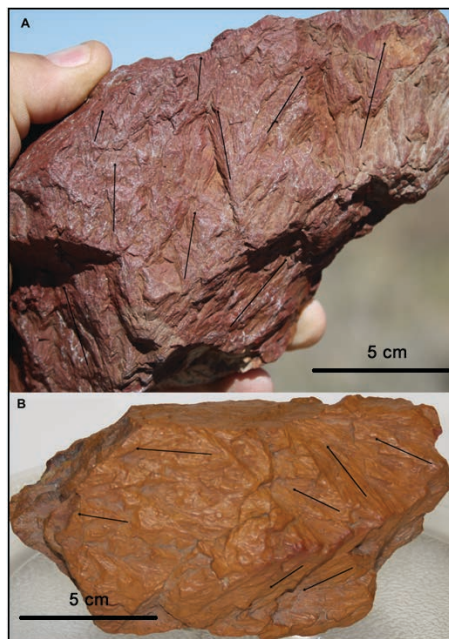


Figure 10. The shatter cones (float) found on the surface of Gum Hole Plain (see Fig. 8). A) a loose cobble found close to LH 125 (18°41'26.57"S, 138°38'59.15"E B) from a region of high abundance on the NE side of the mapped shattercone area (LH 128: 18°40'46.00"S, 138°39'31.20"E). The horsetail striations formed on the exposed surfaces at time of impact suggesting these samples were most likely pre-fractured. Both samples show a change in the direction of the apices of the cones on the differing surfaces. The back surface of B) not shown has apex orientations opposite to the displayed surface.



Figure 11. Dolomite-chert breccia is found within the deformed dolomite annulus surrounding the Gum Hole Plain (a – c) at the Lawn Hill impact site including the inner southern outcrop. a) LH648 b) LH101 (see Fig. 1). c) A large clast (~50 x 50 cm) of Thornton Limestone with fine chert banding. This sample is located at LH620 (see Fig. 1). A photograph showing the entire large clast can be found in the kmz file in the Annulus Breccias folder. d) Breccia within the dolomite at Mt Jennifer is compositionally similar to the other breccias, but the ratio of matrix: clast varies from the main annulus to within the 'dykes'. The Mt Jennifer dykes are the only breccia that contains material from a different lithology (see LHIS.kmz/Mt Jennifer and the Southern Outcrops: LH2 786). Specifically, sandstone clasts that may have originated from the Widdallion Sandstone can be found in a small proportion of the breccia at Mt Jennifer.

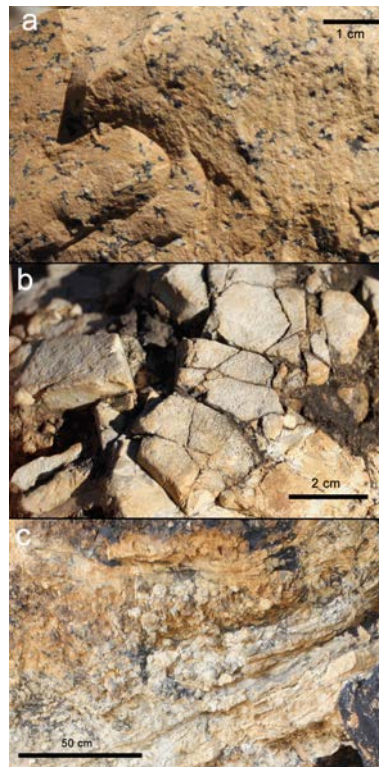


Figure 12. Breccias in the LHIS a) Within the Gum Hole Plain, a brecciated dolomite/calcite breccia, LH183 (see Fig. 8). This material is clast dominant with clasts showing a history of fracturing. b) Mt Jennifer hosts an autoclastic breccia assumed to show significant fracturing of the Widdallion Sandstone located below the dolomite. c) Representative of the siliceous breccia identified as 'Border Waterhole Formation' on previous maps. This image shows the breccia sill injected between layers of sandstone. This suggests the siliceous breccia may have originally been Widdallion Sandstone altered by the impact event. The siliceous breccia lining the inner edge of the dolomite annulus may also have originated as Widdallion Sandstone.

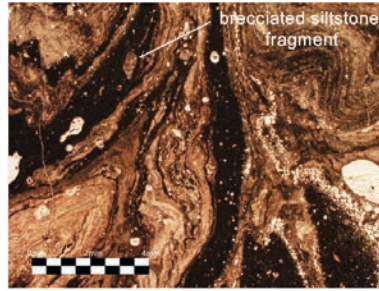


Figure 13. Sample used for  $^{40}\text{Ar}$ - $^{39}\text{Ar}$  dating from JS006 (LH355)  $18^{\circ}40'58.31''\text{S}$ ,  $138^{\circ}39'6.47''\text{E}$ . This PPL image shows the dark convoluted and contorted fluidal melt domain with the embedded siltstone breccia fragments (labelled).

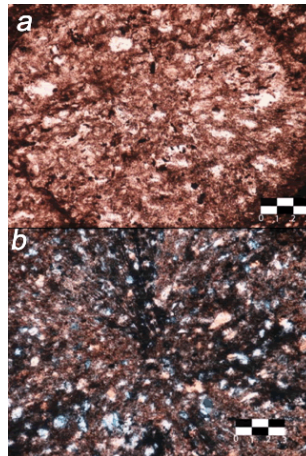


Figure 14. Sample JS023  $18^{\circ}41'31.89''\text{S}$ ,  $138^{\circ}39'0.55''\text{E}$  used for  $^{40}\text{Ar}$ - $^{39}\text{Ar}$  AR dating. a) and b) are PPL and XPL images respectively of a single k-feldspar spherule. **The spherule fills most of the field of view;** scale is in mm.

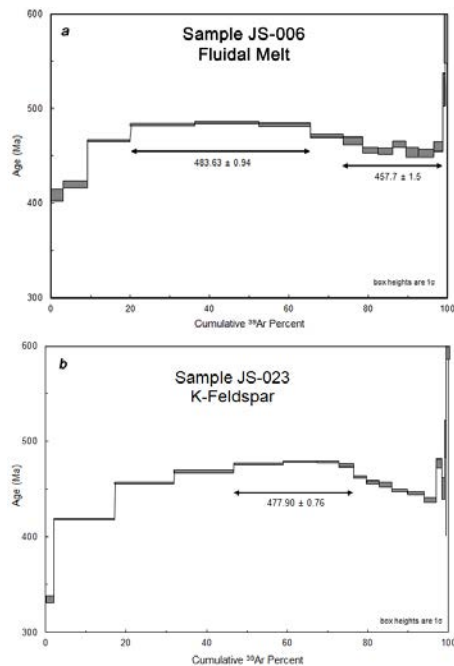


Figure 15. Step heating diagrams. Representative age spectrums of the two samples analyzed. a) JS006 is fluidal melt domain found in the central drill core LH355. b) JS023 located within float material (see Fig. 8 this study and LHIS.kmz/Geochronology). Detailed geochronological analysis details can be found in Table 1.

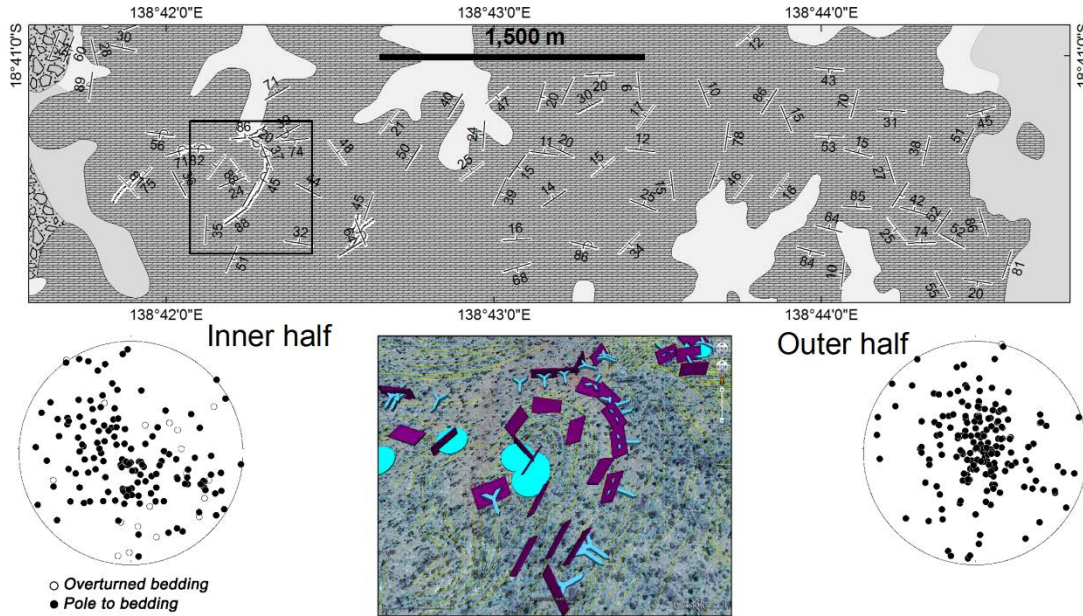


Figure 16: Detailed mapping of the eastern strip ( Fig. 1). Selected bedding measurements, representative of the localized deformation, are shown. Overturning is more common in the inner region – see Inner half stereonet. The inset shows the bedding surfaces (rectangles) with the associated younging (arrows) superimposed on the Google Earth topography with disks marking localities of breccia. Analyses of the sub-divided bedding data i.e. inner and outer sections do not reveal a preferred bedding orientation. All stereoplots are equal area, lower hemisphere plots of poles to bedding.

- Bureau of Mineral Resources (Cartographer). (1982). Geology of the Lawn Hill Region.
- Glikson, M., Golding, S. D., & Southgate, P. N. (2006). Thermal Evolution of the Ore-Hosting Isa Superbasin: Central and Northern Lawn Hill Platform. *Economic Geology*, 101(6), 1211-1229. doi: 10.2113/gsecongeo.101.6.1211
- Lindsay, J., & Brasier, M. (2006). Impact craters as biospheric microenvironments, Lawn Hill Structure, Northern Australia. *Astrobiology*, 6(2), 348-363. doi: 10.1089/ast.2006.6.348
- Lisle, R. J. (1985). The use of the orientation tensor for the description and statistical testing of fabrics. *Journal of Structural Geology*, 7(1), 115-117. doi: 10.1016/0191-8141(85)90119-1
- Salisbury, J. A., Tomkins, A. G., & Schaefer, B. F. (2008). New insights into the size and timing of the Lawn Hill impact structure: relationship to the Century Zn – Pb deposit. *Australian Journal of Earth Sciences*, 55(4), 587-603.
- Shoemaker, E. M., & Shoemaker, C. S. (1996). The Proterozoic impact record of Australia. *AGSO Journal of Australian Geology & Geophysics*, 16, 379-398.
- State of Queensland DNRM. (2011). Rock Unit Surface - Lawn Hill. Retrieved 3 Mar, 2014, from <https://webgis.dme.qld.gov.au/webgis/webqmin/viewer.htm>
- Stewart, A., & Mitchell, K. (1987). Shatter cones at the Lawn Hill circular structure, northwestern Queensland: presumed astrobleme. *Australian Journal of Earth Sciences*, 34(4), 477-485. doi: 10.1080/08120098708729427
- Szulg, S. A. (1992). *The stratigraphic reconstruction of a mega-breccia : a sedimentological study of the south western corner of the Lawn Hill Outlier*. (B Sc (Hons)), James Cook University, Townsville, Qld.,
- Vollmer, F. W. (1990). An application of eigenvalue methods to structural domain analysis. *Geological Society of America Bulletin*, 102(6), 786-791. doi: 10.1130/0016-7606(1990)102<0786:aaemt>2.3.co;2